NASA/TM–2010-216191

Comparison of Comet Enflow and VA One Acoustic-to-Structure Power Flow Predictions

Ferdinand W. Grosveld
Lockheed Martin, Langley Research Center, Hampton, Virginia

Noah H. Schiller and Randolph H. Cabell
Langley Research Center, Hampton, Virginia

February 2010

NASA STI Program . . . in Profile

Since its founding, NASA has been dedicated to the advancement of aeronautics and space science. The NASA scientific and technical information (STI) program plays a key part in helping NASA maintain this important role.

The NASA STI program operates under the auspices of the Agency Chief Information Officer. It collects, organizes, provides for archiving, and disseminates NASA's STI. The NASA STI program provides access to the NASA Aeronautics and Space Database and its public interface, the NASA Technical Report Server, thus providing one of the largest collections of aeronautical and space science STI in the world. Results are published in both non-NASA channels and by NASA in the NASA STI Report Series, which includes the following report types:

- TECHNICAL PUBLICATION. Reports of completed research or a major significant phase of research that present the results of NASA programs and include extensive data or theoretical analysis. Includes compilations of significant scientific and technical data and information deemed to be of continuing reference value. NASA counterpart of peer-reviewed formal professional papers, but having less stringent limitations on manuscript length and extent of graphic presentations.

- TECHNICAL MEMORANDUM. Scientific and technical findings that are preliminary or of specialized interest, e.g., quick release reports, working papers, and bibliographies that contain minimal annotation. Does not contain extensive analysis.

- CONTRACTOR REPORT. Scientific and technical findings by NASA-sponsored contractors and grantees.

- CONFERENCE PUBLICATION. Collected papers from scientific and technical conferences, symposia, seminars, or other meetings sponsored or co-sponsored by NASA.

- SPECIAL PUBLICATION. Scientific, technical, or historical information from NASA programs, projects, and missions, often concerned with subjects having substantial public interest.

- TECHNICAL TRANSLATION. English-language translations of foreign scientific and technical material pertinent to NASA's mission.

Specialized services also include creating custom thesauri, building customized databases, and organizing and publishing research results.

For more information about the NASA STI program, see the following:

- Access the NASA STI program home page at *http://www.sti.nasa.gov*

- E-mail your question via the Internet to help@sti.nasa.gov

- Fax your question to the NASA STI Help Desk at 443-757-5803

- Phone the NASA STI Help Desk at 443-757-5802

- Write to:
  NASA STI Help Desk
  NASA Center for AeroSpace Information
  7115 Standard Drive
  Hanover, MD 21076-1320

NASA/TM–2010-216191

Comparison of Comet Enflow and VA One Acoustic-to-Structure Power Flow Predictions

Ferdinand W. Grosveld
Lockheed Martin, Langley Research Center, Hampton, Virginia

Noah H. Schiller and Randolph H. Cabell
Langley Research Center, Hampton, Virginia

National Aeronautics and
Space Administration

Langley Research Center
Hampton, Virginia 23681-2199

February 2010

Available from:

NASA Center for AeroSpace Information
7115 Standard Drive
Hanover, MD 21076-1320
443-757-5802

TABLE OF CONTENTS

LIST OF TABLES

LIST OF FIGURES

INTRODUCTION

Finite Element Analysis (FEA), Boundary Element Analysis (BEA) and Statistical Energy Analysis (SEA) have been used for decades to analyze vibro-acoustic problems and have matured to the point that reliable predictions can be expected cognizant of the limitations of each method. These prediction tools have been validated for many structurally and/or acoustically excited aerospace, automotive, shipbuilding, and architectural structures in anechoic, reverberant and in-situ acoustic environments. It is generally accepted that the discrete FEA and BEA numerical analyses are applicable towards the low end of the frequency scale, where the individual modal response is dominant. SEA is applied at frequencies where the modal density and the modal overlap are high. The predictions of the vibro-acoustic response made by the FEA and SEA analysis tools were compared with structural and acoustic measurements on a floor-equipped, composite cylinder in References 1-6. The 3.658 m long, filament wound composite cylinder is 1.676 m in diameter and is stiffened by composite frames and longerons. The floor is located 0.544 m above the bottom of the cylinder. The cylinder was originally developed to resemble a composite aircraft fuselage for impact dynamics and acoustic transmission verification (Reference 7).

Since the vibro-acoustic research on the composite cylinder in the 1980s (References 1-6) new measurement equipment, improved experimental tools, and increased data storage have become available to enhance the experimental characterization of a structure such as the composite cylinder. Innovative hybrid analysis and prediction tools have emerged to take advantage of both finite element modeling and statistical analysis. A new set of measurements and predictions of the vibro-acoustic response of the composite cylinder is being pursued to validate these new analysis tools and enhance the physical understanding of the problem. Comet Enflow from Comet Technology Corporation is a commercially available, high frequency vibroacoustic analysis software based on the Energy Finite Element Analysis (EFEA) and Energy Boundary Element Analysis (EBEA). The EFEA is based on deriving governing differential equations in terms of energy density variables and then employing a finite element approach for numerically solving them. In the EFEA, both the structural and acoustic domains are modeled using finite elements and at the interface of geometric and material discontinuities, joint elements based on power flow continuity across the junction are utilized. In this method the same FEA mesh used for structural and acoustic low frequency analysis can be used for the high frequency solutions. In a program managed by the NASA Langley Research Center Structural Acoustics Branch, EFEA as implemented in Comet Enflow is being validated for the floor-equipped composite cylinder by comparing the EFEA vibroacoustic response predictions with SEA and experimental results. The SEA predictions are made using the commercial software program VA One from ESI Group. Early in this program a number of discrepancies became apparent in the Enflow predicted response for the power flow from an acoustic space to a structural subsystem that needed to be investigated first and this research is the subject of this publication. The power flow anomalies were studied for a simple cubic, a rectangular and a cylindrical structural model connected to an acoustic cavity. The current investigation focuses on three specific discrepancies between the Comet Enflow and the VA One predictions: the Enflow power transmission coefficient relative to the VA One coupling loss factor; the importance of the accuracy of the acoustic modal density formulation used within Enflow; and the recommended use of fast solvers in Comet Enflow. The frequency region of interest for this study covers the one-third octave bands with center frequencies from 16 Hz to 4000 Hz.

POWER TRANSMISSION COEFFICIENT

The Comet Enflow prediction program was found to use an acoustic-to-structure power transmission coefficient half in value of the transmission coefficient suggested in the literature. A derivation of the

power transmission coefficient is offered in this section and will be compared with the Comet Enflow implementation and with the equation found in the literature.

The acoustic-to-structure power transmission coefficient, τ_{as}, between an air-filled acoustic cavity and a plate structure was found in the literature as derived by Bitsie in Reference 8 and was cited in a study on the parametric design sensitivity analysis of high frequency structural-acoustic problems using the energy finite element method (References 9 and 10)

$$\tau_{as} = \beta_{sa} \frac{c^2}{c_{ph}} \frac{\sigma_{rad}}{fh} \tag{1}$$

where c is the speed of sound in air, c_{ph} is the characteristic phase speed of the plate, σ_{rad} is the radiation efficiency of the plate, f is the frequency, h is the thickness of the plate structure, and β_{sa} is the ratio of the acoustic and the structural characteristic impedances

$$\beta_{sa} = \frac{\rho c}{\rho_s c_{ph}} \tag{2}$$

The radiation efficiency of the plate is related to the density ratio for the acoustic medium and structural material, the wavenumber k, the plate thickness h, and the radiation loss factor η_{rad}

$$\sigma_{rad} = \frac{\rho}{\rho_s} kh\eta_{rad} \tag{3}$$

Assuming that the group speed c_{gf} in the plate is twice the phase speed c_{ph}

$$c_{gf} = 2c_{ph} \tag{4}$$

results in the following expression for the acoustic-structure power transmission coefficient (Reference 8)

$$\tau_{as} = \frac{8\pi c^2 \eta_{rad}}{c_{gf}^2} \tag{5}$$

However, the Comet Enflow prediction program is using

$$\tau_{as} = \frac{4\pi c^2 \eta_{rad}}{c_{gf}^2} \tag{6}$$

as confirmed by manual calculations for a simple case.

The following derivation for the acoustic-to-structure power transmission coefficient, as a function of the radiation coupling loss factor, is offered to verify that the formulation in the Comet Enflow program is correct. The sound power of a diffuse acoustic field incident on one side of a plate is given by[11]

$$\Pi_{inc} = \frac{\overline{p_0^2}}{4\rho c} A \tag{7}$$

where $\overline{p_0^2}$ is the mean square acoustic pressure, ρ_0 is the density of air, c_0 is the speed of sound in air and A is the plate surface area. The sound power Π_{inc} incident on the plate is partially reflected (Π_{refl}) and the remaining power (the power flowing into the plate) sets the plate into vibration. Damping in the plate dissipates some of that power (Π_{diss}) while part of the remaining power is radiated by the plate back into the fluid (air) on the source side of the plate (Π_{rad}) and another part is radiated from the other side of the plate (Π_t). The power flow balance can then be expressed as (Figure 1).

$$\Pi_{inc} - \Pi_{refl} = \Pi_{diss} + \Pi_{rad} + \Pi_t \tag{8}$$

or in coefficients relative to the incident sound power Π_{inc}

$$1 - \tau_{refl} = \gamma_{diss} + \tau_{rad} + \tau_t \tag{9}$$

where τ_{refl} is the power reflection coefficient, γ_{diss} is the plate power dissipation coefficient and τ_{rad} is the source side surface plate power radiation coefficient, which is equal in magnitude to the power transmission coefficient τ_t. When combining Equations (7), (8), and (9), the power flowing into the plate becomes

$$\Pi_{inc} - \Pi_{refl} = (\gamma_{diss} + 2\tau_t)\frac{\overline{p_0^2}}{4\rho c} A \tag{10}$$

Assuming that the plate power dissipation coefficient is much smaller than the power radiation coefficient

$$\gamma_{diss} << 2\tau_t \tag{11}$$

yields the following expression for the power flow from the acoustic space to the structure

$$\Pi_{as} = \Pi_{inc} - \Pi_{refl} = \tau_t \frac{\overline{p_0^2}}{2\rho c} A \tag{12}$$

The coupling loss factor η_{as} between the resonant energies of the acoustic space and the plate is given by[12]

$$\eta_{as} = \frac{\Pi_{as}}{\omega E_a} \tag{13}$$

where ω is the rotational frequency and E_a is the energy in the acoustic space with volume V

$$E_a = \frac{\overline{p_0^2}}{\rho c^2} V \tag{14}$$

Equations (12), (13) and (14) yield

$$\eta_{as} = \frac{2\tau_t A c}{4\omega V} = \frac{\tau_t A c}{2\omega V} \tag{15}$$

The power transmission coefficient then becomes

$$\tau_t = \frac{2\omega V \eta_{as}}{Ac} \tag{16}$$

Reciprocity is defined by[13]

$$\eta_{as} = \frac{n_s(f)}{n_a(f)} \eta_{sa} \tag{17}$$

where n_s is the structural modal density of the plate, n_a is the modal density of the acoustic source space, and η_{sa} is the structure (plate) to acoustic space coupling loss factor. The modal density of the plate is given by[13]

$$n_s(f) = \frac{\omega A}{c_{ph} c_{gf}} \tag{18}$$

where c_{ph} is, again, the phase speed in the plate and c_{gf} is the group speed. The acoustic modal density is defined by[14]

$$n_a(f) = \frac{4\pi V}{c^3} f^2 + \frac{\pi A}{2c^2} f + \frac{P}{8c} \tag{19}$$

where V is the volume, A is the total surface area and P is the total perimeter of the acoustic space.

Combining Equations (9) thru (12) and assuming

$$c_{gf} = 2c_{ph} \tag{20}$$

and

$$\eta_{rad} = \eta_{sa} \tag{21}$$

yields for the power transmission coefficient

$$\tau_t = \frac{4\pi c^2 \eta_{rad}}{c_{gf}^2} \xi \tag{22}$$

where the coefficient ξ is defined by

$$\xi = \frac{\frac{4\pi V}{c^3} f^2}{\frac{4\pi V}{c^3} f^2 + \frac{\pi S}{2c^2} f + \frac{P}{8c}} \tag{23}$$

Equation (22) is the same as Equation (6) used in the Comet Enflow program when the coefficient ξ in Equation (23) is equal to 1, which means that only the volume term of the acoustic modal density

expression in Equation (19) is used in the Comet Enflow problem formulation. The derivation by Bitsie is based on the analysis by Fahy (Reference 15) on the broadband absorption by multi-modal vibration in architectural acoustics. Walls in a building may absorb the sound but will not efficiently radiate sound on both sides of the structure like in the case of a vibrating thin plate.

A simple model consisting of two parallel, opposing thin plates coupled to a cubical acoustic cavity in between (Figure 2) was analyzed to compare the Comet Enflow power transmission coefficient formulations in Equations (5) and (6) with the results from VA One computations on the same model. The plates had aluminum material properties, a length and width of 1 m, and a thickness of 0.008 m. The speed of sound was assumed to be 343 m/s and the density was 1.21 kg/m^3. One of the plates was injected in the center by a unit of power. The SEA model employs three substructures, the two plates and the acoustic cavity (Figure 2). A finite element model consisting of 100 quad elements for each of the plates and 1000 hexagonal elements for the acoustic cavity (Figure 3) was created and imported into the Comet Enflow software program.

The root-mean-square velocity response of the excited plate predicted by SEA inVA One, and by EFEA in Comet Enflow with the power transmission coefficients of Equations (5) and (6) is shown in Figure 4 as a function of the one-third octave band center frequency. Equation (5) is indicated in this figure as having the "8" coefficient found in the literature, while Equation (6) has the "4" coefficient default in Comet Enflow. Close agreement is obtained between the results of both the "4" and the "8" power transmission coefficients indicating that the energy loss due to radiation into the interior acoustic space is negligible relative to the energy present in the flexural vibrations of the plate.

In contrast to the structural response of the plate, Figure 5 shows that the different power transmission coefficients have a profound impact on the averaged sound pressure level inside the acoustic cavity. Below the critical frequency, which was calculated at 1469 Hz, the default "4" power transmission coefficient in Comet Enflow yields results that are 1-3 dB closer to the VA One predictions than the Comet Enflow predictions using the "8" power transmission coefficient found in the literature. However, even the "4" coefficient predictions still substantially deviate (from 1 dB at 400 Hz to more than 6 dB at 100 Hz) from the sound pressure level results obtained using VA One. This deviation will be investigated in the next section. Above the critical frequency reasonable agreement (within 1 dB) is obtained between the "4" and "8" Comet Enflow predictions and VA One.

The root-mean-square velocity predictions for the opposing plate 2 in the plate-cavity-plate model (Figure 2) are shown in Figure 6. The Comet Enflow predictions using the default "4" power transmission coefficient are closer to the VA One results than using the "8" coefficient from the literature.

ACOUSTIC MODAL DENSITY

Comet Enflow uses only the volume related term in Equation (19) corresponding to ξ=1 in Equation (23). However, statistical energy analysis programs like VA One (Reference 16) use also the area and perimeter related terms in their calculations of the acoustic modal density. Figure 7 shows the contributions of the volume term, the area term, the perimeter term and all three combined on the acoustic modal density of the cubical cavity of Figure 2. Including all three terms, rather than only the volume term, affects the acoustic modal density predominantly at the low frequencies. The importance of including all three terms in the modal density Equation (19) was further investigated for a rectangular acoustic cavity (Figure 8), a cylindrical acoustic cavity (Figure 9a) and the upper and lower spaces in a floor-equipped cylinder (Figure 9b and Figure 9c). The acoustic modal density equations were verified by summing the mode counts obtained from analytical and numerical predictions, and experimental modal analysis. The Comet Acoustics Enflow code was amended by the publisher with a capability to include

any of the acoustic modal density terms in Equation (19) by modifying the acoustic element input card {PACOUS id ρ c dac ispdac v s p}, where v is the volume, s is the total surface area and p is the total perimeter of the acoustic cavity.

Rectangular cavity modal frequencies

The longest dimension of the rectangular cavity was 3.658 m, which is equal to the length of the floor-equipped composite cylinder studied in References 1-6. The dimensions of the box were in the ratio of $1:2^{1/3}:4^{1/3}$ as suggested by Bolt in Reference 17 to achieve the best approximation to evenly spaced modes in the acoustic cavity. A finite element model of the box with dimensions 2.304 m by 2.903 m by 3.658 m and consisting of ten hexagonal elements along each direction is depicted in Figure 8a. The acoustic modal frequencies f_n in a hard-walled rectangular cavity can be calculated from (Reference 11)

$$f_{n_x,n_y,n_z} = \frac{c}{2}\sqrt{\left[\frac{n_x}{l}\right]^2 + \left[\frac{n_y}{w}\right]^2 + \left[\frac{n_z}{h}\right]^2} \qquad (24)$$

where c is the speed of sound (343 m/s), n_x, n_y, and n_z are the mode numbers in the x, y, and z directions and l, w and h are the length, width and height of the cavity, respectively. Mode types include axial, tangential and oblique modes having, respectively, two, one and no mode numbers equal to zero. The analytical modal frequencies for the first 72 modes are listed in Table 1 along with the mode type, the length, width and height order and the one-third octave band in which they appear. The total number of modes in each one-third octave band is shown in parentheses.

A numerical modal analysis was performed on the finite element model of Figure 8a using the commercially available Comet Corporation Structural Acoustic Foam Engineering (SAFE) analysis software. Modal frequencies were calculated for all modes up to and including the 400 Hz one-third octave band. The resulting modal frequencies are also listed in Table 1 along with the one-third octave band in which they appear and the number of modes in each band between parentheses. The modal frequencies in each one-third octave band are assigned a different color (Table 1). Not all calculated modal frequencies in the 250 Hz one-third octave bands were identified.

The accuracy of the numerical results was found to be dependent on the eigensystem frequency shift, which is used in the Comet SAFE code to prevent anomalies due to rigid body motion. Choosing a shift of 1 Hz rather than the initial 20 Hz improved the fundamental acoustic frequency prediction by almost 15%, from 43.31 Hz to 46.68 Hz, which is within 0.437% of the 46.88 Hz analytically predicted fundamental modal frequency (Table 1). However, the numerical modal frequencies are underpredicted progressively more with increasing frequency (Table 1), resulting in a significantly higher mode count per one-third octave band than determined by the analytical approach (i.e. 34 modes in the 200 Hz one-third octave band for the numerical computations versus 19 modes for the analytical prediction).

To improve the mode count per one-third octave band for the numerically computed modal frequencies the number of elements in the length, width and height directions of the acoustical cavity were increased to 20 (Figure 8b) and 30 elements (Figure 8c). The results are compared with the analytical mode count in Table 2. Incomplete mode counts in the one-third octave bands are grayed out. Good agreement (within 8%) was obtained in the 250 Hz and lower one-third octave bands for the 30- by 30- by 30- element model. A 40- by 40- by 40-element model was pursued but not enough memory could be allocated for the computations in a 32-bit operating system environment of the Comet SAFE code. Development is underway by the Comet Technology Corporation to upgrade the code to a 64-bit

Microsoft Windows operating system. The number of modes in the hard-walled rectangular acoustic cavity are given by (Reference 11)

$$N(f) = \frac{4\pi V}{3c^3} f^3 + \frac{\pi A}{4c^2} f^2 + \frac{P}{8c} f \qquad (25)$$

Table 3 shows the number of rectangular cavity acoustic modal frequencies in each of the 16 Hz to 4000 Hz one-third octave bands computed with the mode count Equation (25) for the volume term, both the volume and the area terms, and for all three terms. An SEA model was created in the SEA program VA One from ESI Group North America (Reference 16) and the mode counts for the volume term, both the volume and the area terms, and for all three terms were output from the program and are listed in Table 1 as well, with identical results as expected. The mode count Equation (25) is compared in Table 4 with the analytical and numerical mode counts. Excellent agreement with the analytical mode count was obtained for the mode count equation having three terms for all one-third octave bands below and including the 630 Hz one-third octave band. The equation result was within 2.6 % of the analytical prediction in the 250 Hz one-third octave band while the volume-term-only equation was off by 35%. In Table 5 the number of modes from zero up to the highest frequency in each one-third octave band is compared for the analytical and numerical mode counts and the calculations using Equation (25). Excellent agreement was obtained between the three-term equation and the analytical mode count over the frequency range from zero to the highest frequency in the 250 Hz one-third octave band (within 1.2%) compared with a 52% discrepancy between the volume-term-only equation and the analytical mode count. In addition, the numerical mode count agreed well with the analytical number of modes as the difference was within 5% for the thirty-element per dimension model over the same frequency range. From zero up to the highest frequency in the 200 Hz one-third octave band the difference is only 2.2% for the thirty-element per dimension model. This suggests that using an element length of maximal 0.1219 m provides a good approximation of the mode count using the numerical Comet SAFE code. The number of elements per acoustic wavelength is tabulated in Table 6 for the 10-, 20-, and 30-element rectangular cavity models. A minimum of approximately eleven to fourteen elements per acoustic wavelength are thus recommended for a reasonably accurate mode count using the Comet SAFE program to perform the modal analysis.

Cylindrical cavity modal frequencies

The acoustic resonance frequencies in a hard-walled cylindrical cavity of length l and radius r are given by[19]

$$f_{j,k,q} = \frac{c}{2\pi} \sqrt{\frac{\lambda_{j,k}^2}{r^2} + \frac{(\pi q)^2}{l^2}} \qquad (26)$$

where j, k and q are the radial, azimuthal and longitudinal mode numbers, c is the speed of sound, and the values λ_{jk} are the roots of $J_n'(\pi\lambda_{jk}) = 0$ where J_n is the Bessel function of order n. The values λ_{jk} are summarized[21] in Table 7. The analytical acoustic resonance frequencies of Equation (26) were validated by comparison with the experimental and computed resonance frequencies of a 1.2192 m long cylindrical cavity with a radius of 0.254 m in Reference 18. Reasonable agreement was obtained between the calculated and measured resonance frequencies as shown in Table 8.

Acoustic resonance frequencies were then calculated for the acoustic cavity of the composite cylinder in References 1-6, which is 3.658 m long and features a radius of 1.676 m. Modal frequencies were calculated for all modes up to and including the 315 Hz one-third octave band. The first 67 analytical modes of the cylinder cavity are listed in Table 9.

A finite element model consisting of hexagonal elements was developed for the cavity of the composite cylinder in References 1-6. A hidden line graphic of the acoustic cavity model is shown in Figure 9. The largest element dimension along the longitudinal axis is 0.127 m which is comparable to the maximal element length (0.1219 m) in the thirty-element ractangular box model (Table 6). This suggests that predictions using the Comet SAFE modal analysis program should provide a good approximation of the numerical modal frequencies and corresponding mode shapes of the cylinder cavity up to and including the 250 Hz one-third octave band. The first 67 modes predicted in Comet SAFE were identified by mode shape. Figure 10 shows a phase plot of the numerical fundamental longitudinal acoustic mode (0,0,1) in the cylinder cavity at 46.9 Hz (Table 7) where the difference in color indicates locations that are 180° out-of-phase. The numerical fundamental radial acoustic mode (1,0,0) at 246.2 Hz in the cylinder cavity is depicted in Figure 11. Phase plots of the numerical fundamental azimuthal acoustic mode (0,1,0) at 119.6 Hz and the same mode shape at a relative 90° phase rotation (119.7 Hz) in the cylinder cavity are shown in Figure 12. The phase rotation of the same azimuthal mode shape depends on the azimuthal mode order *k*

$$phase\ rotation = \frac{\pi}{2k} \tag{27}$$

A phase plot of the (0,2,4) azimuthal-longitudinal acoustic mode at 266.6 Hz (Figure 13a) shows the same mode shape at a 45° relative phase rotation (Figure 13b). The phase plot of the (0,3,1) azimuthal-longitudinal acoustic mode at 272.3 Hz in Figure 14a shows the same mode shape at a 30° relative phase rotation (272.8 Hz) in Figure 14b. The first 67 numerical modal frequencies are tabulated in Table 9 for phase rotation, and radial, azimuthal and longitudinal order. Table 9 shows that the analytically and numerically predicted modal frequencies are quite close in the 250 Hz one-third octave band. For example, the analytical prediction of mode number 34 with mode shape (0,3,1) at 277.6 Hz is only 1.8% higher than the numerically predicted mode at 272.8 Hz. Analytical modal frequencies high in the 315 Hz one-third octave band are typically up to 4% higher than the numerical modal frequencies.

Table 10 shows the number of analytical and numerical cylinder acoustic modes in each one-third octave band compared to the mode count equation containing the volume, the volume and area, and the volume, area and perimeter terms. Since the analytical and numerical predictions of the modal frequencies were pretty close (<1.8% for the 250 Hz one-third octave band and lower) the summation of the modal frequencies in each one-third octave band is almost the same. In the 250 Hz one-third octave band the analytical mode count is 15 while the numerical mode count equals 16. The mode count using Equation (25) equals 15 when all three terms are included. The mode count using this equation with only the volume term is calculated to be 9 which is 6 modes, or 40%, less than the result of the analytical calculation. The mode count in the rectangular cavity, using Equation (25), was a good approximation for the number of analytical and numerical modes in each individual one-third octave band even at the lower frequencies as the rectangular cavity had dimensions such that the modes were rather evenly distributed over the frequency spectrum.[17] However, the modes of the cylinder are not evenly distributed over the frequency range of interest and the agreement between the mode counts from the Equation (25) calculations and the analytical and numerical results vary as shown in Table 10 for band numbers 17 through 23. The agreement is much better when considering all the modes from zero frequency up to the highest frequency of each one-third octave band. This is demonstrated in Table 11 where the mode count equation compares much better with the analytical predictions in the frequency bands 17 through 23. The calculations using the mode count equation have been compared with the output from the VA One SEA program using a statistical energy analysis model of the same cylindrical acoustic cavity. Results for one, two and three terms are shown in Table 12 for the mode counts in each individual one-third octave frequency band and in Table 13 for the region from zero frequency up to the highest frequency in each one-third octave band. As expected the results are basically the same, since the mode count Equation (25) is used in VA One.

Cavity modal frequencies above and below the cylinder floor

Since no analytical solution is available for the calculation of the resonance frequencies in the acoustic cavities above and below the floor of the cylinder in References 1-6 a numerical modal analysis was performed in Comet SAFE. The finite element model in Figure 9 was partitioned to create models for the cavities above and below the cylinder floor as shown in Figure 15. The element size was exactly the same as used in the modal analysis predictions for the entire cylinder cavity suggesting that predictions are reasonably accurate up to and including the 250 Hz one-third octave band. Modal frequencies were calculated for all modes up to and including the 500 Hz one-third octave band. The first 34 numerically predicted modal frequencies were identified according to mode shapes of radial, azimuthal and longitudinal orders. The modal frequencies in the acoustic cavity above the floor are listed in Table 14 while the modal frequencies for the bottom cavity are tabulated in Table 15. Figure 16 shows a phase plot of the numerical fundamental longitudinal (0,0,1) acoustic mode at 46.9 Hz in the cavity above the floor (Table 14) and in the cavity below the floor (Table 15). A phase plot of the numerical fundamental radial (1,0,0) acoustic mode at 160.3 Hz in the cavity above the floor (Table 14) and at 351.2 Hz in the cavity below the floor (Table 15) is depicted in Figure 17. A phase plot of the numerical fundamental azimuthal (0,1,0) acoustic mode at 113.8 Hz in the cylinder cavity above the floor (Table 14) and at 137.5 Hz in the cavity below the floor (Table 15) is shown in Figure 18. Finally, Figure 19 shows a phase plot of the (0,2,4) azimuthal- longitudinal acoustic mode at 282.0 Hz in the cylinder cavity above the floor (Table 14) and at 296.8 Hz in the cavity below the floor (Table 15). The numerically calculated modal frequencies were summed in each one-third octave band 16 Hz – 500 Hz and are compared in Table 16 and Table 17 to the results of the mode count Equation (25) with the volume term, the volume and area terms and the volume, area and perimeter terms. Reasonably good agreement (within 8%) was obtained for the cavity above the floor with the three-term mode count equation, where the numerical predictions resulted in 12 modes for the 250 Hz one-third octave band while the three-term mode count equation produced 11 modes (Table 16). However, the volume-term-only mode count equation had only 7 modes, strongly underpredicting (42%) the numerical calculations. Similar comparisons were obtained for the cavity below the floor as evidenced in Table 17. Good comparison between the numerical results and the three-term mode count equation for the cavity above the floor were also obtained when summing all the modes from zero to the highest frequency in each one-third octave band as shown in Table 18. The volume-term-only equation underpredicted the numerical results by more than 50% in all one-third octave bands below 400 Hz containing modes. Similar results were obtained for the cavity below the floor as shown in Table 19.

Cubical acoustic cavity bounded by two plates

It was shown in the previous sections that the modal density in a rectangular cavity, a cylinder cavity or the cavities above and below of a floor-equipped cylinder were much more accurate using the volume, the area and the perimeter terms in the mode count Equation (25) than using the volume term only as in the Comet Enflow predictions. The Comet Enflow predictions for the cubical acoustic cavity (Figure 3) were more than 6 dB below the VA One predictions (Figure 5) for the same plate-cavity-plate model subject to unit power input (Figure 2). The Comet Enflow predictions were repeated with all three terms using the correction factor ξ in Equation (23). The results are shown in Figure 20. Excellent agreement is obtained as the corrected Comet Enflow predictions are within 1.0 dB of the VA One predictions over the entire 100 Hz to 4000 Hz one-third octave band frequency range. The VA One and Comet Enflow root-mean-square velocity response predictions for the receiving plate 2 in Figure 6 were repeated as well using the correction factor ξ in Equation (23). The new Comet Enflow calculations were within 5.0% of the SEA predictions over the entire 100 Hz to 4000 Hz one-third octave band frequency range except for the 1600 Hz one-third octave band containing the critical frequency at 1469 Hz.

ACOUSTIC MEASUREMENTS

The Comet Safe predictions for the acoustic modal parameters in the composite cylinder above the floor were verified by comparing them with previously measured[1] acoustic resonance frequencies in the same cavity of the composite cylinder described in References 1-6. Some of the measurements results from Reference 1 are reported here and compared with the Comet Safe numerically computed modal frequencies listed in Table 14. The modal characteristics of the cylinder interior cavity above the floor are defined by acoustic modal frequencies, mode shapes and loss factors. To determine these modal parameters sound pressure levels were conducted throughout the interior of the cylinder bounded by the floor, the endcaps and the cylinder shell.[1] An I-beam located along the axis of the cylinder supported a boom on which six one-half inch condenser microphones were mounted. The boom slides along the center beam which can be rotated over 220 degrees to facilitate acoustic measurements at different azimuthal positions for any desired cross section. The microphones were located at integral multiples of five inches from the centerline. One of the microphones was located between the center beam and the floor.

Modal frequencies

The interior of the cylinder was subjected to white noise from a loudspeaker source located in a corner where the cylinder shell meets the floor and the front endcap.[1] Bode spectra were obtained for each of the six microphones at eleven evenly spaced, longitudinal locations with the boom oriented in the vertical plane. In addition, Bode spectra were obtained at fifteen azimuthal positions of the boom (15° intervals) at a cross-section 3.35 m from the front endcap. Modal frequencies and mode shapes were identified from peak sound pressure levels in the frequency spectra and the equal sound pressure level contour plots (Figure 22). Adjacent contour lines represent a 3 dB change in root-mean-square sound pressure level. The heavy lines in Figure 22 indicate the nodal lines of the measured acoustic mode shapes, where the root-mean-square pressure is a minimum and pressure on either side are out-of-phase.

The experimental modal frequencies are compared with the Comet SAFE numerically calculated modal frequencies (Table 14) in Table 20. Reasonably good agreement was obtained as most of the numerically predicted modal frequencies are within 3.7% of the experimental values. Only three of the seventeen modal frequencies listed in Table 20 show a higher difference (up to 6.3%).

Experimental acoustic loss factors

The acoustic loss factor η_{aa} of an enclosure[19] can be calculated as a function of the frequency f and the reverberation time T_{60}

$$\eta_{aa} = \frac{2.2}{f\,T_{60}} \tag{28}$$

The integrated impulse method was used[1] to measure the reverberation time in the cavity above the floor. The results in each one-third octave band were averaged over six horizontal and six vertical microphone locations 0.3 m from the front endcap.[1] The loss factors averaged over all microphone locations are tabulated for the 31.5 Hz to 500 Hz one-third octave bands in Table 21 and for the 1000 Hz to 4000 Hz octave bands in Table 22.

OPTIONAL ITERATIVE SOLVERS

The EFEA computations in this study were executed in the Comet Enflow program with the default Gaussian Elimination solver. In addition, Comet Enflow offers two iterative solver options, the Incomplete LU (ITER LU) and the Diagonal Scaling (DIAG) solvers (Reference 21) to solve large problems more efficiently and save computation time. The preconditioner index, the tolerance of iteration (default value of 1.0E-6) and the maximum iteration number (default value equals the number degrees of freedom, DOF) can be specified for each solver. Care must be taken in the use of the iterative solvers as for small size problems, where the system matrix is small, the results to the problem may not converge and large discrepancies may occur. This is illustrated in Figure 23 and Figure 24 where the solutions from the Gaussian Elimination, the iterative LU solver and the Diagonal Scaling solver are compared with the SEA results for the sound pressure level in the cavity and the root-mean-square velocity of plate 2 in the cube problem of Figure 2 has been used. It is recommended to first use the Gaussian Elimination solver on a representative problem and use the accuracy of the results as a reference for all subsequent calculations.

CONCLUSIONS

A derivation was provided for the relation between the acoustic-to-structure Energy Finite Element Analysis (EFEA) power transmission coefficient and the Statistical Energy Analysis (SEA) coupling loss factor confirming the proper calculations by the Comet Enflow program and contradicting equations published in References 8-10.

The modal parameters of a cubic, rectangular and cylindrical cavity were analytically predicted, and numerically calculated using the commercially available Comet Corporation Structural Acoustic Foam Engineering (SAFE) analysis software. The results were summed to obtain the mode count in each one-third octave band. The element size of the acoustic cavity finite element model was linked to the acoustic wavelength to determine the highest one-third octave frequency band in which the numerical predictions differed less than 5% of the analytical predictions. The analytical and numerical results were compared to the mode count equation with the volume, the volume and the area, and the volume, the area and the perimeter terms. It was shown that the three-term mode count equation gave much better results than the volume-term-only formulation. This was illustrated by the three-term equation being within 2.6 % of the analytical prediction for the rectangular acoustic cavity in the 250 Hz one-third octave band while the volume-term-only equation was off by 35%. For the cylindrical acoustic cavity the three-term mode count equation calculation in the 250 Hz one-third octave band was exactly the same as the number of modes predicted analytically, while the mode count by the volume-term-only equation was 40% less. The same element size as the cylindrical cavity finite element model was used for the numerical computation of the modal parameters in the acoustic cavities above and below the floor of the composite cylinder, thereby expecting similar accuracy in the numerical predictions. The summation of the numerical modal frequencies in the acoustic cavity above the cylinder floor compared reasonably well with the three-term mode count equation (within 8%) in the 250 Hz one-third octave band, while the volume-term-only mode count equation was off by 42%. The three-term mode count equation was also used for the Comet Enflow sound pressure level predictions in the cubic acoustic cavity of a plate-cavity-plate system, where a unit power input was applied to one of the plates. The predictions were within 1 dB of the SEA results over the entire frequency range of interest 100 Hz to 400 Hz. The discrepancy between the volume-only-term equation and the VA One predictions had been as large as 6 dB at 100 Hz.

Numerically calculated modal frequencies in Comet SAFE were compared with acoustic modal frequencies measured in the cavity above the floor of the composite cylinder during studies performed in the 1980s. Reasonably good agreement was obtained as most of the numerical modal frequencies were within 3.7% of the experimental values. Only three of the seventeen modal frequencies differed more (up to 6.3%).

Use of the Incomplete LU (ITER LU) and the Diagonal Scaling (DIAG) iterative solver options was found to lead to significant errors for small size problems, where the system matrix is small and the results to the problem may not converge. It is recommended to first use the Gaussian Elimination solver on a representative problem and use the accuracy of the results as a reference for all subsequent calculations.

REFERENCES

1. Grosveld, F. W., and Beyer, T. B., Modal Characteristics of a Stiffened Cylinder with Open and Closed End Conditions. AIAA 86-1908, AIAA 10th Aeroacoustics Conference, Seattle, Washington, July 9-11, 1986.
2. Beyer, T. B. and Grosveld, F. W., Validation of an Interior Noise Prediction Model for a Composite Cylinder. AIAA-87-0529, AIAA 25th Aerospace Sciences Meeting, Reno, Nevada, January 12-15, 1987.
3. Grosveld, F. W. and Beyer, T. B., Vibratory Response of a Stiffened, Floor-Equipped, Composite Cylinder. *Proceedings of the 5th International Modal Analysis Conference*, London, England, April 6-9, 1987, pp. 812-820.
4. Grosveld, F. W., Sullivan, B. and Marulo, F., Aircraft Interior Noise Prediction Using a Structural Acoustic Analogy in NASTRAN Modal Synthesis. *Proceedings of the 6th International Modal Analysis Conference*, Orlando, FL, February 1-4, 1988, pp. 1191-1198.
5. Beyer, T. and Silcox, R., Noise Transmission of a Large Scale Composite Fuselage Model. AIAA-90-3965, AIAA 13th Aeroacoustics Conference, Tallahassee, Florida, October 22-24, 1990.
6. Grosveld, Ferdinand W., Noise Reduction of a Composite Cylinder Subjected to Random Acoustic Excitation. AIAA-89-1049, AIAA 12th Aeroacoustics Conference, San Antonio, TX, April 10-12, 1989.
7. Jackson, A. C., Balena, F. J., Labarge, W. L., Pei, G., Pitman, W. A. and Wittlin, G., Transport Composite Fuselage Technology: Impact Dynamics and Acoustic Transmission. NASA-CR-4035, December 1986.
8. Bitsie, Fernando, The Structural-Acoustic Energy Finite Element Method and Energy Boundary Element Method. Ph.D. Dissertation, Mechanical Engineering Department, Purdue University, Lafayette, IN, 1996.
9. Dong Jun, Choi, Kyung K., Wang, Aimin, Zhang, Weiguo, Vlahopoulos, Nickolas, Parametric Design Sensitivity Analysis of High Frequency Structural–Acoustic Problems Using Energy Finite Element Method. *International Journal for Numerical Methods in Engineering*, 2005, 62: 83–121
10. Choi, K. K., Dong, J., Vlahopoulos, N., Wang, A., Zhang, W., "Parametric Design Sensitivity Analysis of High Frequency Structural-Acoustic Problems Using Energy Finite Element Method", DETC/DAC-48753, ASME 2003 Design Engineering Technical Conferences and Computers and Information in Engineering Conference, September 02 –06, 2003, Chicago, IL.
11. Bies, D. A. and Hansen, C. H., *Engineering Noise Control - Theory and Practice*, New York: Spon Press, Third Edition, 2003.
12. Keane, A. J. and Price W. G., *Statistical Energy Analysis: An Overview, with Applications in Structural Dynamics.* Cambridge University Press, 1994.

13. Lyon, Richard, H. and DeJong, Richard G., *Theory and Application of Statistical Energy Analysis.* Boston: Butterworth-Heinemann, Second Edition, 1995.
14. Maa, D. Y., The Distribution of Eigentones in a Rectangular Chamber at Lower Frequency Ranges. *J. Acous. Soc. Am.* 12, 39, 1940.
15. Fahy, F., *Sound and Structural Vibration: Radiation, Transmission, and Response.* Academic Press, London, 1985.
16. VA One User's Guide. ESI Group North America, San Diego, 2007.
17. Bolt R. H., Note on the Normal Frequency Statistics in Rectangular Rooms. J. Acoust. Soc. Am. 18(1) 130-133. (1946).
18. Pope, L. D.; Rennison, D. C.; Willis, C. M.; Mayes, W. H., Development and Validation of Preliminary Analytical Models for Aircraft Interior Noise Prediction. *Journal of Sound and Vibration*, vol. 82, June 22, 1982, p. 541-575.
19. Beranek, L. L. and Vér, I. L., *Noise and Vibration Control Engineering: Principles and Applications.* Second Edition, John Wiley & Sons, Cambridge, Massachusetts, USA, 2007.
20. Birkin, P. R., Leighton, T. G., Power, J. F., Simpson, M. D., Vinçotte, A. M. L., and Joseph, P. F., Experimental and Theoretical Characterization of Sonochemical Cells. Part 1. Cylindrical Reactors and their Use to Calculate the Speed of Sound in Aqueous Solutions. *J. Phys. Chem. A*, 107, 2003, pp. 306-320.
21. Comet Enflow User's Manual. Comet Technology Corporation, Ann Arbor, MI, 2007.

TABLES

Table 1. Analytically and numerically predicted acoustic modal frequencies for the first 72 modes in a 3.658 m by 2.903 m by 2.304 m rectangular air-filled cavity (c=343 m/s; ρ=1.21 kg/m^3).

Mode Number	Mode Type	Length Order	Width Order	Height Order	Analytical Modal Frequency [Hz]	One-third Octave Band [Hz] (# modes)	Numerical Modal Frequency [Hz]	One-third Octave Band [Hz] (# modes)
1	Axial Length	1	0	0	46.88	50 (1)	46.68	50 (1)
2	Axial Width	0	1	0	59.08	63 (1)	58.83	63 (1)
3	Axial Height	0	0	1	74.44	80 (3)	74.12	80 (3)
4	Tangential L,W	1	1	0	75.42		74.49	
5	Tangential L,H	1	0	1	87.97		86.88	
6	Axial Length	2	0	0	93.77	100 (4)	92.23	100 (4)
7	Tangential W,H	0	1	1	95.03		93.86	
8	Oblique L,W,H	1	1	1	105.97		103.80	
9	Tangential L,W	2	1	0	110.83		107.74	
10	Axial Width	0	2	0	118.15	125 (6)	116.22	125 (6)
11	Tangential L,H	2	0	1	119.72		116.24	
12	Tangential L,W	1	2	0	127.12		123.80	
13	Oblique L,W,H	2	1	1	133.50		128.37	
14	Tangential W,H	0	2	1	139.65		135.76	
15	Axial Length	3	0	0	140.65		135.50	
16	Oblique L,W,H	1	2	1	147.31	160 (12)	141.91	160 (16)
17	Axial Height	0	0	2	148.87		146.43	
18	Tangential L,W	2	2	0	150.84		143.57	
19	Tangential L,W	3	1	0	152.55		145.07	
20	Tangential L,H	1	0	2	156.08		152.10	
21	Tangential L,H	3	0	1	159.13		151.00	
22	Tangential W,H	0	1	2	160.16		155.99	
23	Oblique L,W,H	1	1	2	166.89		161.07	
24	Oblique L,W,H	2	2	1	168.21		158.41	
25	Oblique L,W,H	3	1	1	169.74		159.27	
26	Tangential L,H	2	0	2	175.94		167.46	
27	Axial Width	0	3	0	177.23		170.74	
28	Tangential L,W	1	3	0	183.33	200 (19)	174.81	
29	Tangential L,W	3	2	0	183.69		169.83	
30	Oblique L,W,H	2	1	2	185.59		174.98	
31	Axial Length	4	0	0	187.53		175.43	
32	Tangential W,H	0	2	2	190.06		180.90	200 (34)
33	Tangential W,H	0	3	1	192.23		182.80	
34	Oblique L,W,H	1	2	2	195.76		184.67	
35	Tangential L,W	4	1	0	196.62		181.49	

Table 1 (continued). Analytically and numerically predicted acoustic modal frequencies for the first 72 modes in a 3.658 m by 2.903 m by 2.304 m rectangular air-filled cavity (c=343 m/s; ρ=1.21 kg/m3).

Mode Number	Mode Type	Length Order	Width Order	Height Order	Analytical Modal Frequency [Hz]	One-third Octave Band [Hz}	Numerical Modal Frequency [Hz]	One-third Octave Band [Hz]
36	Oblique L,W,H	1	3	1	197.86		186.34	
37	Oblique L,W,H	3	2	1	198.20		181.14	
38	Tangential L,W	2	3	0	200.51		186.10	
39	Tangential L,H	4	0	1	201.77		185.75	
40	Tangential L,H	3	0	2	204.81		188.91	
41	Oblique L,W,H	4	1	1	210.24		191.21	
42	Oblique L,W,H	2	2	2	211.93		195.19	
43	Oblique L,W,H	3	1	2	213.16		194.68	
44	Oblique L,W,H	2	3	1	213.88		196.23	
45	Tangential L,W	4	2	0	221.65		198.02	
46	Axial Height	0	0	3	223.31		215.13	
47	Tangential L,W	3	3	0	226.26	250	202.45	
48	Tangential L,H	1	0	3	228.18		217.73	
49	Tangential W,H	0	1	3	230.99		220.25	
50	Tangential W,H	0	3	2	231.46		213.99	
51	Oblique L,W,H	4	2	1	233.82		206.24	
52	Axial Length	5	0	0	234.42		211.05	
53	Oblique L,W,H	1	1	3	235.70		222.64	
54	Oblique L,W,H	1	3	2	236.16		216.35	
55	Axial Width	0	4	0	236.31		221.06	
56	Oblique L,W,H	3	2	2	236.44		210.54	
57	Oblique L,W,H	3	3	1	238.19		210.72	
58	Tangential L,H	4	0	2	239.44		212.89	
59	Tangential L,W	1	4	0	240.91		223.04	
60	Tangential L,W	5	1	0	241.75		214.76	
61	Tangential L,H	2	0	3	242.19		225.11	
62	Tangential L,H	5	0	1	245.95		217.89	
63	Oblique L,W,H	4	1	2	246.62		216.97	
64	Tangential W,H	0	4	1	247.75		228.69	
65	Oblique L,W,H	2	1	3	249.30		229.44	
66	Oblique L,W,H	2	3	2	249.73		223.04	
67	Oblique L,W,H	1	4	1	252.15		230.43	
68	Tangential W,H	0	2	3	252.64		234.49	
69	Oblique L,W,H	5	1	1	252.95		221.30	
70	Tangential L,W	2	4	0	254.23		228.70	
71	Oblique L,W,H	1	2	3	256.95		236.33	
72	Tangential L,W	4	3	0	258.03		221.33	

Table 2. Number of analytical rectangular cavity acoustic modal frequencies in each one-third octave band compared to the numerical mode count for 10, 20 and 30 elements in each perpendicular geometric direction.

Band Number	One-third Octave Band [Hz}	Lower Frequency [Hz}	Upper Frequency [Hz}	Analytical Mode Count	Numerical Mode Count Ten Elements	Numerical Mode Count Twenty Elements	Numerical Mode Count Thirty Elements
12	16	14.1	17.8	0	0	0	0
13	20	17.8	22.4	0	0	0	0
14	25	22.4	28.2	0	0	0	0
15	31.5	28.2	35.5	0	0	0	0
16	40	35.5	44.7	0	0	0	0
17	50	44.7	56.2	1	1	1	1
18	63	56.2	70.8	1	1	1	1
19	80	70.8	89.1	3	3	3	3
20	100	89.1	112	4	4	4	4
21	125	112	141	6	6	6	6
22	160	141	178	12	16	12	12
23	200	178	224	19	34	20	20
24	250	224	282	39	272	48	42
25	315	282	355	74	709	96	83
26	400	355	447	142	63	223	161
27	500	447	562	265	0		
28	630	562	708	515	0		
29	800	708	891	864	0		
30	1000	891	1122	845	0		
31	1250	1122	1413	212	0		
32	1600	1413	1778	0	0		
33	2000	1778	2239	0	0		
34	2500	2239	2818	0	0		
35	3150	2818	3548	0	0		
36	4000	3548	4467	0	0		

Table 3. Number of rectangular cavity acoustic modal frequencies in each one-third octave band computed by the mode count equation and the equivalent SEA equation containing the volume; the volume and area; and the volume, area and perimeter terms.

Band Number	One-third Octave Band [Hz}	Lower Frequency [Hz}	Upper Frequency [Hz}	Mode Count Equation Volume Term	Mode Count Equation Volume +Area	Mode Count Equation Volume +Area +Perimeter	SEA Volume Term	SEA Volume +Area	SEA Volume +Area +Perimeter
12	16	14.1	17.8	0	0	0	0	0	0
13	20	17.8	22.4	0	0	0	0	0	0
14	25	22.4	28.2	0	0	0	0	0	0
15	31.5	28.2	35.5	0	0	0	0	0	0
16	40	35.5	44.7	0	0	0	0	0	0
17	50	44.7	56.2	0	1	1	0	1	1
18	63	56.2	70.8	1	1	1	1	1	1
19	80	70.8	89.1	1	2	2	1	2	2
20	100	89.1	112	2	3	4	2	3	4
21	125	112	141	4	6	6	4	6	6
22	160	141	178	8	11	12	8	11	12
23	200	178	224	15	21	21	15	21	21
24	250	224	282	29	38	38	29	38	38
25	315	282	355	57	71	72	57	71	72
26	400	355	447	116	138	139	116	138	139
27	500	447	562	224	259	260	224	259	260
28	630	562	708	450	505	507	450	505	507
29	800	708	891	905	994	995	905	994	995
30	1000	891	1122	1780	1920	1922	1780	1920	1922
31	1250	1122	1413	3495	3716	3719	3495	3716	3719
32	1600	1413	1778	7169	7523	7526	7169	7523	7526
33	2000	1778	2239	14127	14687	14691	14127	14687	14691
34	2500	2239	2818	27694	28573	28578	27694	28573	28578
35	3150	2818	3548	55383	56779	56785	55383	56779	56785
36	4000	3548	4467	112345	114576	114584	112345	114576	114584

Table 4. Number of analytical and numerical rectangular cavity acoustic modes in each one-third octave band compared to the mode count equation containing the volume; the volume and area; and the volume, area and perimeter terms.

Band Number	One-third Octave Band [Hz}	Lower Frequency [Hz}	Upper Frequency [Hz}	Analytical Mode Count	Numerical Mode Count Thirty Elements	Mode Count Equation Volume Term	Mode Count Equation Volume +Area	Mode Count Equation Volume +Area +Perimeter
12	16	14.1	17.8	0	0	0	0	0
13	20	17.8	22.4	0	0	0	0	0
14	25	22.4	28.2	0	0	0	0	0
15	31.5	28.2	35.5	0	0	0	0	0
16	40	35.5	44.7	0	0	0	0	0
17	50	44.7	56.2	1	1	0	1	1
18	63	56.2	70.8	1	1	1	1	1
19	80	70.8	89.1	3	3	1	2	2
20	100	89.1	112	4	4	2	3	4
21	125	112	141	6	6	4	6	6
22	160	141	178	12	12	8	11	12
23	200	178	224	19	20	15	21	21
24	250	224	282	39	42	29	38	38
25	315	282	355	74	83	57	71	72
26	400	355	447	142	161	116	138	139
27	500	447	562	265		224	259	260
28	630	562	708	515		450	505	507
29	800	708	891	864		905	994	995
30	1000	891	1122	845		1780	1920	1922
31	1250	1122	1413	212		3495	3716	3719
32	1600	1413	1778	0		7169	7523	7526
33	2000	1778	2239	0		14127	14687	14691
34	2500	2239	2818	0		27694	28573	28578
35	3150	2818	3548	0		55383	56779	56785
36	4000	3548	4467	0		112345	114576	114584

Table 5. Number of analytical and numerical rectangular cavity acoustic modes between 0 Hz and the highest frequency in each one-third octave band compared to the mode count equation containing the volume; the volume and area; and the volume, area and perimeter terms.

Band Number	One-third Octave Band [Hz}	Lower Frequency [Hz}	Upper Frequency [Hz}	Analytical Mode Count	Numerical Mode Count Thirty Elements	Mode Count Equation Volume Term	Mode Count Equation Volume +Area	Mode Count Equation Volume +Area +Perimeter
12	16	14.1	17.8	0	0	0	0	0
13	20	17.8	22.4	0	0	0	0	0
14	25	22.4	28.2	0	0	0	0	0
15	31.5	28.2	35.5	0	0	0	0	0
16	40	35.5	44.7	0	0	0	0	0
17	50	44.7	56.2	1	1	0	1	1
18	63	56.2	70.8	2	2	0	2	2
19	80	70.8	89.1	5	5	1	4	4
20	100	89.1	112	9	9	3	7	8
21	125	112	141	15	15	7	13	14
22	160	141	178	27	27	14	25	25
23	200	178	224	46	47	28	45	46
24	250	224	282	85	89	56	84	84
25	315	282	355	159	172	113	156	157

Table 6. Number of elements per acoustic wavelength for the 10-, 20-, and 30-element rectangular cavity models.

One-third Octave Band [Hz]	Wavelength [m]	Number of elements/wavelength Ten-element Model (Element length=0.3658 m)	Twenty-element Model (Element length=0.1829 m)	Thirty-element Model (Element length=0.1219 m)
16	21.44	58.6	117.2	175.8
20	17.15	46.9	93.8	140.7
25	13.72	37.5	75.0	112.5
31.5	10.89	29.8	59.5	89.3
40	8.58	23.4	46.9	70.3
50	6.86	18.8	37.5	56.3
63	5.44	14.9	29.8	44.7
80	4.29	11.7	23.4	35.2
100	3.43	9.4	18.8	28.1
125	2.74	7.5	15.0	22.5
160	2.14	5.9	11.7	17.6
200	1.72	4.7	9.4	14.1
250	1.37	3.8	7.5	11.3
315	1.09	3.0	6.0	8.9
400	0.86	2.3	4.7	7.0

Table 7. Values of λ_{jk}.for the acoustic resonance modes in a cylindrical cavity.

						j					
k	0	1	2	3	4	5	6	7	8	9	10
0	0.00	1.84	3.05	4.20	5.32	6.42	7.50	8.58	9.66	10.72	11.78
1	3.83	5.33	6.71	8.03	9.28	10.52	11.73	12.94	14.12	15.30	16.46
2	7.02	8.54	9.97	11.35	12.68	13.99	15.27	16.54	17.78	19.02	20.24
3	10.17	11.71	13.17	14.59	15.96	17.31	18.64	19.96	21.24	22.52	23.78
4	13.34	14.88	16.36	17.80	19.20	20.58	21.94	23.28	24.60	25.90	27.18
5	16.48	18.02	19.52	20.98	22.42	23.82	25.20	26.56	27.90	29.22	30.54
6	19.62	21.18	22.68	24.16	25.60	27.02	28.42	29.80	31.16	32.52	33.86

Table 8. Calculated and experimental acoustic modal frequencies (Ref. 19) for a 1.2192 m long cylindrical air-filled cavity (c=343 m/s and ρ=1.21 kg/m3) with a radius of 0.254 m compared with analytical predictions.

Radial Order	**Azimuthal Order**	**Longitudinal Order**	**Analytical Modal Frequency [Hz]**	**Experimental Modal Frequency (Ref. 19) [Hz]**	**Calculated Modal Frequency (Ref. 19) [Hz]**
0	0	1	140.7	142.6	140.7
0	0	2	281.3	282.8	281.4
0	1	0	395.7	400.0	395.7
0	1	1	420.0		420.0
0	0	3	422.0	426.0	422.1
0	1	2	485.5	490.8	485.6
0	0	4	562.7	568	562.8
0	1	3	578.5	585	578.6
0	2	0	656.4	641	656.4
0	2	1	671.3	670	671.3
0	1	4	687.9	685	688.0
0	0	5	703.3	709	703.4

Table 9. Analytically and numerically predicted acoustic modal frequencies for the first 67 acoustic modes of a 3.658 m long cylindrical air-filled cavity (c=343 m/s and ρ=1.21 kg/m3) with a radius of 0.8382 m.

Mode Number	Radial Order	Azimuthal Order	Longitudinal Order	Phase Rotation	Analytical Modal Frequency [Hz]	Numerical Modal Frequency [Hz]
1	0	0	1		46.5	46.9
2	0	0	2		93.8	93.6
3	0	1	0		119.9	119.6
4	0	1	0	90	119.9	119.7
5	0	1	1		128.8	128.2
6	0	1	1	90	128.8	128.3
7	0	0	3		140.7	140.0
8	0	1	2		152.2	151.1
9	0	1	2	90	152.2	151.2
10	0	1	3		184.8	182.7
11	0	1	3	90	184.8	182.8
12	0	0	4		187.5	186.0
13	0	2	0		198.9	197.2
14	0	2	0	45	198.9	197.3
15	0	2	1		204.4	202.3
16	0	2	1	45	204.4	202.4
17	0	2	2		219.9	216.9
18	0	2	2	45	219.9	216.9
19	0	1	4		222.6	219.1
20	0	1	4	90	222.6	219.2
21	0	0	5		234.4	231.5
22	0	2	3		243.6	239.0
23	0	2	3	45	243.6	239.2
24	1	0	0		249.6	246.2
25	1	0	1		253.9	250.2
26	0	1	5		263.3	257.8
27	0	1	5	90	263.3	258.0
28	1	0	2		266.6	261.6
29	0	2	4		273.4	266.6
30	0	2	4	45	273.4	266.9
31	0	3	0		273.6	268.7
32	0	3	0	30	273.6	269.3
33	0	3	1		277.6	272.3
34	0	3	1	30	277.6	272.8

Table 9 (continued). Analytically and numerically predicted acoustic modal frequencies for the first 67 acoustic modes of a 3.658 m long cylindrical air-filled cavity (c=343 m/s; ρ=1.21 kg/m3) with a radius of 0.8382 m.

Mode Number	Radial Order	Azimuthal Order	Longitudinal Order	Phase Rotation	Analytical Modal Frequency [Hz]	Numerical Modal Frequency [Hz]
35	0	0	6		281.3	276.3
36	1	0	3		286.5	279.4
37	0	3	2		289.2	282.6
38	0	3	2	30	289.2	283.2
39	0	1	6		305.8	297.7
40	0	1	6	90	305.8	297.8
41	0	2	5		307.4	297.9
42	0	2	5	45	307.4	298.3
43	0	3	3		307.6	298.9
44	0	3	3	30	307.6	299.5
45	1	0	4		312.2	302.4
46	0	3	4		331.7	320.1
47	0	0	7		328.2	320.2
48	0	3	4	30	331.7	320.7
49	1	0	5		342.4	329.1
50	0	2	6		344.5	331.5
51	0	2	6	45	344.5	332.0
52	1	1	0		347.2	334.9
53	1	1	0	45	347.2	335.1
54	1	1	1		350.4	337.5
55	1	1	1	45	350.4	337.7
56	0	1	7		349.4	337.8
57	0	1	7	45	349.4	338.0
58	0	4	0		346.3	338.2
59	0	4	0	22.5	346.3	338.9
60	0	4	1		349.5	340.9
61	0	4	1	22.5	349.5	341.5
62	1	1	2		359.7	345.0
63	0	3	5		360.3	345.1
64	1	1	2	90	359.7	345.2
65	0	3	5	30	360.3	345.7
66	0	4	2		358.8	348.6
67	0	4	2	22.5	358.8	349.3

Table 10. Number of analytical and numerical cylinder acoustic modes in each one-third octave band compared to the mode count equation containing the volume, the volume and area, and the volume, area and perimeter terms.

Band Number	One-third Octave Band [Hz}	Lower Frequency [Hz}	Upper Frequency [Hz}	Analytical Mode Count	Numerical Mode Count	Mode Count Equation Volume Term	Mode Count Equation Volume +Area	Mode Count Equation Volume +Area +Perimeter
12	16	14.1	17.8	0	0	0	0	0
13	20	17.8	22.4	0	0	0	0	0
14	25	22.4	28.2	0	0	0	0	0
15	31.5	28.2	35.5	0	0	0	0	0
16	40	35.5	44.7	0	0	0	0	0
17	50	44.7	56.2	1	1	0	0	0
18	63	56.2	70.8	0	0	0	0	1
19	80	70.8	89.1	0	0	0	1	1
20	100	89.1	112	1	1	1	1	2
21	125	112	141	5	5	1	2	3
22	160	141	178	2	2	2	4	5
23	200	178	224	11	11	5	8	8
24	250	224	282	15	16	9	14	15
25	315	282	355	26	31	19	26	27
26	400	355	447			37	49	50
27	500	447	562			74	92	93
28	630	562	708			149	178	179
29	800	708	891			295	342	343
30	1000	891	1122			591	664	667
31	1250	1122	1413			1181	1297	1300
32	1600	1413	1778			2346	2530	2534
33	2000	1778	2239			4696	4989	4993
34	2500	2239	2818			9348	9811	9816
35	3150	2818	3548			18677	19412	19419
36	4000	3548	4467			37272	38436	38444

Table 11. Number of analytical and numerical cylindrical cavity acoustic modes between 0 Hz and the highest frequency in each one-third octave band compared to the mode count equation containing the volume, the volume and area, and the volume, area and perimeter terms.

Band Number	One-third Octave Band [Hz}	Lower Frequency [Hz}	Upper Frequency [Hz}	Analytical Mode Count	Numerical Mode Count	Mode Count Equation Volume Term	Mode Count Equation Volume +Area	Mode Count Equation Volume +Area +Perimeter
12	16	14.1	17.8	0	0	0	0	0
13	20	17.8	22.4	0	0	0	0	0
14	25	22.4	28.2	0	0	0	0	0
15	31.5	28.2	35.5	0	0	0	0	0
16	40	35.5	44.7	0	0	0	0	0
17	50	44.7	56.2	1	1	0	0	1
18	63	56.2	70.8	1	1	0	1	1
19	80	70.8	89.1	1	1	0	1	2
20	100	89.1	112	2	2	1	3	4
21	125	112	141	7	7	2	5	6
22	160	141	178	9	9	4	9	11
23	200	178	224	20	20	9	17	19
24	250	224	282	35	36	18	31	33
25	315	282	355	61	67	37	57	60
26	400	355	447			74	106	110
27	500	447	562			148	198	203
28	630	562	708			297	376	383
29	800	708	891			592	718	726
30	1000	891	1122			1183	1382	1393
31	1250	1122	1413			2364	2680	2692
32	1600	1413	1778			4710	5210	5226
33	2000	1778	2239			9407	10199	10220
34	2500	2239	2818			18755	20010	20036
35	3150	2818	3548			37432	39422	39454
36	4000	3548	4467			74703	77858	77899

Table 12. Number of cylindrical cavity acoustic modal frequencies in each one-third octave band computed by the mode count equation and the equivalent SEA equation containing the volume, the volume and area, and the volume, area and perimeter terms.

Band Number	One-third Octave Band [Hz}	Lower Frequency [Hz}	Upper Frequency [Hz}	Mode Count Equation Volume Term	Mode Count Equation Volume +Area	Mode Count Equation Volume +Area +Perimeter	SEA Volume Term	SEA Volume +Area	SEA Volume +Area +Perimeter
12	16	14.1	17.8	0	0	0	0	0	0
13	20	17.8	22.4	0	0	0	0	0	0
14	25	22.4	28.2	0	0	0	0	0	0
15	31.5	28.2	35.5	0	0	0	0	0	0
16	40	35.5	44.7	0	0	0	0	0	0
17	50	44.7	56.2	0	0	0	0	0	0
18	63	56.2	70.8	0	0	1	0	0	1
19	80	70.8	89.1	0	1	1	0	1	1
20	100	89.1	112	1	1	2	1	1	2
21	125	112	141	1	2	3	1	2	3
22	160	141	178	2	4	5	2	4	5
23	200	178	224	5	8	8	5	8	8
24	250	224	282	9	14	15	9	14	14
25	315	282	355	19	26	27	18	25	26
26	400	355	447	37	49	50	37	49	49
27	500	447	562	74	92	93	72	90	91
28	630	562	708	149	178	179	146	175	176
29	800	708	891	295	342	343	294	341	342
30	1000	891	1122	591	664	667	580	653	655
31	1250	1122	1413	1181	1297	1300	1142	1257	1260
32	1600	1413	1778	2346	2530	2534	2348	2532	2536
33	2000	1778	2239	4696	4989	4993	4633	4925	4929
34	2500	2239	2818	9348	9811	9816	9093	9550	9555
35	3150	2818	3548	18677	19412	19419	18200	18927	18933
36	4000	3548	4467	37272	38436	38444	36946	38108	38116

Table 13. Number of cylindrical cavity acoustic modal frequencies between 0 Hz and the highest frequency in each one-third octave band computed by the mode count equation and the equivalent SEA equation containing the volume, the volume and area, and the volume, area and perimeter terms.

Band Number	One-third Octave Band [Hz}	Lower Frequency [Hz}	Upper Frequency [Hz}	Mode Count Equation Volume Term	Mode Count Equation Volume +Area	Mode Count Equation Volume +Area +Perimeter	SEA Volume Term	SEA Volume +Area	SEA Volume +Area +Perimeter
12	16	14.1	17.8	0	0	0	0	0	0
13	20	17.8	22.4	0	0	0	0	0	0
14	25	22.4	28.2	0	0	0	0	0	0
15	31.5	28.2	35.5	0	0	0	0	0	0
16	40	35.5	44.7	0	0	0	0	0	0
17	50	44.7	56.2	0	0	0	0	0	0
18	63	56.2	70.8	0	0	1	0	0	1
19	80	70.8	89.1	0	1	1	0	1	1
20	100	89.1	112	1	1	2	1	1	2
21	125	112	141	1	2	3	1	2	3
22	160	141	178	2	4	5	2	4	5
23	200	178	224	5	8	8	5	8	8
24	250	224	282	9	14	15	9	14	14
25	315	282	355	19	26	27	18	25	26
26	400	355	447	37	49	50	37	49	49
27	500	447	562	74	92	93	72	90	91
28	630	562	708	149	178	179	146	175	176
29	800	708	891	295	342	343	294	341	342
30	1000	891	1122	591	664	667	580	653	655
31	1250	1122	1413	1181	1297	1300	1142	1257	1260
32	1600	1413	1778	2346	2530	2534	2348	2532	2536
33	2000	1778	2239	4696	4989	4993	4633	4925	4929
34	2500	2239	2818	9348	9811	9816	9093	9550	9555
35	3150	2818	3548	18677	19412	19419	18200	18927	18933
36	4000	3548	4467	37272	38436	38444	36946	38108	38116

Table 14. Numerically predicted modal frequencies for the first 34 modes of the acoustic cavity above the cylinder floor (top).

Mode Number	Radial Order	Azimuthal Order	Longitudinal Order	Numerical Modal Frequency [Hz]
1	0	0	1	46.9
2	0	0	2	93.6
3	0	1	0	113.8
4	0	1	1	122.9
5	0	0	3	140.0
6	0	1	2	146.6
7	1	0	0	160.3
8	1	0	1	166.6
9	0	1	3	179.1
10	1	0	2	184.3
11	0	0	4	186.0
12	1	0	3	210.3
13	0	1	4	216.2
14	0	2	0	219.1
15	1	1	0	222.8
16	0	2	1	223.6
17	1	1	1	227.2
18	0	0	5	231.5
19	0	2	2	236.6
20	1	1	2	239.9
21	1	0	4	241.6
22	0	1	5	255.4
23	0	2	3	256.6
24	1	1	3	259.6
25	0	0	6	276.3
26	1	0	5	276.3
27	2	2	0	278.6
28	2	2	1	281.9
29	0	2	4	282.0
30	1	1	4	284.6
31	2	2	2	291.5
32	0	1	6	295.7
33	2	2	3	306.8
34	0	2	5	311.1

Table 15. Numerically predicted modal frequencies for the first 34 modes of the acoustic cavity below the cylinder floor (bottom).

Mode Number	Radial Order	Azimuthal Order	Longitudinal Order	Numerical Modal Frequency [Hz]
1	0	0	1	46.9
2	0	0	2	93.6
3	0	1	0	137.5
4	0	0	3	140.0
5	0	1	1	145.1
6	0	1	2	165.6
7	0	0	4	186.0
8	0	1	3	194.9
9	0	1	4	229.2
10	0	0	5	231.5
11	0	2	0	237.7
12	0	2	1	241.9
13	0	2	2	254.0
14	0	1	5	266.5
15	0	2	3	272.7
16	0	0	6	276.3
17	0	2	4	296.8
18	0	1	6	305.1
19	0	0	7	320.2
20	0	2	5	324.6
21	0	3	0	329.6
22	0	3	1	332.3
23	0	3	2	340.3
24	0	1	7	344.3
25	1	0	0	351.2
26	0	3	3	353.2
27	1	0	1	353.8
28	0	2	6	355.1
29	1	0	2	361.4
30	0	0	8	363.2
31	0	3	4	370.2
32	1	0	3	373.6
33	0	1	8	383.6
34	0	2	7	387.2

Table 16. Number of numerical top cylinder cavity acoustic modes in each one-third octave band compared to the mode count equation containing the volume, the volume and area, and the volume, area and perimeter terms.

Band Number	One-third Octave Band [Hz}	Lower Frequency [Hz}	Upper Frequency [Hz}	Numerical Mode Count	Mode Count Equation Volume Term	Mode Count Equation Volume +Area	Mode Count Equation Volume +Area +Perimeter
12	16	14.1	17.8	0	0	0	0
13	20	17.8	22.4	0	0	0	0
14	25	22.4	28.2	0	0	0	0
15	31.5	28.2	35.5	0	0	0	0
16	40	35.5	44.7	0	0	0	0
17	50	44.7	56.2	1	0	0	0
18	63	56.2	70.8	0	0	0	0
19	80	70.8	89.1	0	0	1	1
20	100	89.1	112	1	0	1	1
21	125	112	141	3	1	2	2
22	160	141	178	3	2	3	4
23	200	178	224	8	3	6	6
24	250	224	282	12	7	11	11
25	315	282	355	27	13	20	21
26	400	355	447	47	27	37	38
27	500	447	562	192	53	69	70
28	630	562	708		107	133	134
29	800	708	891		213	253	255
30	1000	891	1122		425	490	492
31	1250	1122	1413		850	952	955
32	1600	1413	1778		1689	1851	1854
33	2000	1778	2239		3381	3638	3642
34	2500	2239	2818		6730	7136	7141
35	3150	2818	3548		13447	14091	14097
36	4000	3548	4467		26834	27855	27863

Table 17. Number of numerical bottom cylinder cavity acoustic modes in each one-third octave band compared to the mode count equation containing the volume, the volume and area, and the volume, area and perimeter terms.

Band Number	One-third Octave Band [Hz}	Lower Frequency [Hz}	Upper Frequency [Hz}	Numerical Mode Count	Mode Count Equation Volume Term	Mode Count Equation Volume +Area	Mode Count Equation Volume +Area +Perimeter
12	16	14.1	17.8	0	0	0	0
13	20	17.8	22.4	0	0	0	0
14	25	22.4	28.2	0	0	0	0
15	31.5	28.2	35.5	0	0	0	0
16	40	35.5	44.7	0	0	0	0
17	50	44.7	56.2	1	0	0	0
18	63	56.2	70.8	0	0	0	0
19	80	70.8	89.1	0	0	0	1
20	100	89.1	112	1	0	1	1
21	125	112	141	2	0	1	1
22	160	141	178	2	1	2	2
23	200	178	224	2	1	3	3
24	250	224	282	8	3	5	6
25	315	282	355	11	5	10	10
26	400	355	447	24	10	18	18
27	500	447	562	45	21	32	33
28	630	562	708		42	59	61
29	800	708	891		83	111	112
30	1000	891	1122		166	210	212
31	1250	1122	1413		331	401	404
32	1600	1413	1778		657	769	772
33	2000	1778	2239		1315	1493	1497
34	2500	2239	2818		2618	2899	2904
35	3150	2818	3548		5231	5677	5683
36	4000	3548	4467		10438	11145	11153

Table 18. Number of numerical top cylinder cavity acoustic modes between 0 Hz and the highest frequency in each one-third octave band compared to the mode count equation containing the volume, the volume and area, and the volume, area and perimeter terms.

Band Number	One-third Octave Band [Hz}	Lower Frequency [Hz}	Upper Frequency [Hz}	Numerical Mode Count	Mode Count Equation Volume Term	Mode Count Equation Volume +Area	Mode Count Equation Volume +Area +Perimeter
12	16	14.1	17.8	0	0	0	0
13	20	17.8	22.4	0	0	0	0
14	25	22.4	28.2	0	0	0	0
15	31.5	28.2	35.5	0	0	0	0
16	40	35.5	44.7	0	0	0	0
17	50	44.7	56.2	1	0	0	1
18	63	56.2	70.8	1	0	0	1
19	80	70.8	89.1	1	0	1	2
20	100	89.1	112	2	0	2	3
21	125	112	141	5	1	4	5
22	160	141	178	8	3	7	9
23	200	178	224	16	6	13	15
24	250	224	282	28	13	24	27
25	315	282	355	55	26	44	47

Table 19. Number of numerical bottom cylinder cavity acoustic modes between 0 Hz and the highest frequency in each one-third octave band compared to the mode count equation containing the volume, the volume and area, and the volume, area and perimeter terms.

Band Number	One-third Octave Band [Hz}	Lower Frequency [Hz}	Upper Frequency [Hz}	Numerical Mode Count	Mode Count Equation Volume Term	Mode Count Equation Volume +Area	Mode Count Equation Volume +Area +Perimeter
12	16	14.1	17.8	0	0	0	0
13	20	17.8	22.4	0	0	0	0
14	25	22.4	28.2	0	0	0	0
15	31.5	28.2	35.5	0	0	0	0
16	40	35.5	44.7	0	0	0	0
17	50	44.7	56.2	1	0	0	0
18	63	56.2	70.8	1	0	0	1
19	80	70.8	89.1	1	0	0	1
20	100	89.1	112	2	0	1	2
21	125	112	141	4	0	2	3
22	160	141	178	6	1	4	5
23	200	178	224	8	2	7	9
24	250	224	282	16	5	12	15
25	315	282	355	27	10	22	25

Table 20. Measured acoustic modal frequencies[6] for the top cylinder cavity compared with numerical predictions.

Radial Order	Azimuthal Order	Longitudinal Order	Measured Modal Frequency[6] [Hz]	Numerical Modal Frequency [Hz]	Difference [%]
0	0	1	47	46.9	-0.3
0	0	2	94	93.6	-0.4
0	1	1	121	122.9	1.5
0	0	3	143	140.0	-2.1
0	1	2	150	146.6	-2.3
1	0	0	171	160.3	-6.3
0	1	3	183	179.1	-2.1
0	0	4	191	186.0	-2.6
1	0	3	216	210.3	-2.6
0	2	1	230	223.6	-2.8
0	0	5	239	231.5	-3.1
1	0	4	249	241.6	-3.0
0	2	3	266	256.6	-3.5
0	0	6	287	276.3	-3.7
0	2	4	295	282.0	-4.4
0	2	5	328	311.1	-5.1
0	3	3	350	337.1	-3.7

Table 21. Acoustic loss factor averaged over six vertical and six horizontal microphone positions in a cross-section above the floor 0.3 m from the front endcap as function of one-third octave band.

Band Number	One-third Octave Band [Hz}	Lower Frequency [Hz}	Upper Frequency [Hz}	Averaged Acoustic Loss Factors
15	31.5	28.2	35.5	0.105
16	40	35.5	44.7	0.137
17	50	44.7	56.2	0.038
18	63	56.2	70.8	0.075
19	80	70.8	89.1	0.099
20	100	89.1	112	0.031
21	125	112	141	0.047
22	160	141	178	0.030
23	200	178	224	0.017
24	250	224	282	0.009
25	315	282	355	0.017
26	400	355	447	0.010
27	500	447	562	0.007

Table 22. Acoustic loss factor averaged over six vertical and six horizontal microphone positions in a cross-section above the floor 0.3 m from the front endcap as function of octave band.

Octave Band [Hz}	Lower Frequency [Hz}	Upper Frequency [Hz}	Averaged Acoustic Loss Factors
1000	708	1413	0.005
2000	1413	2818	0.002
4000	2818	5650	0.001

FIGURES

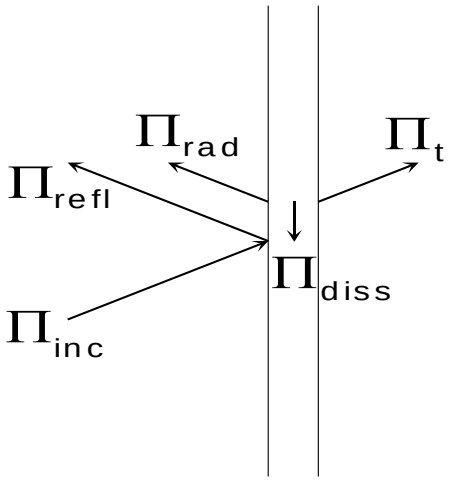

Figure 1. Incident, reflected, radiated, transmitted and dissipated power coefficients.

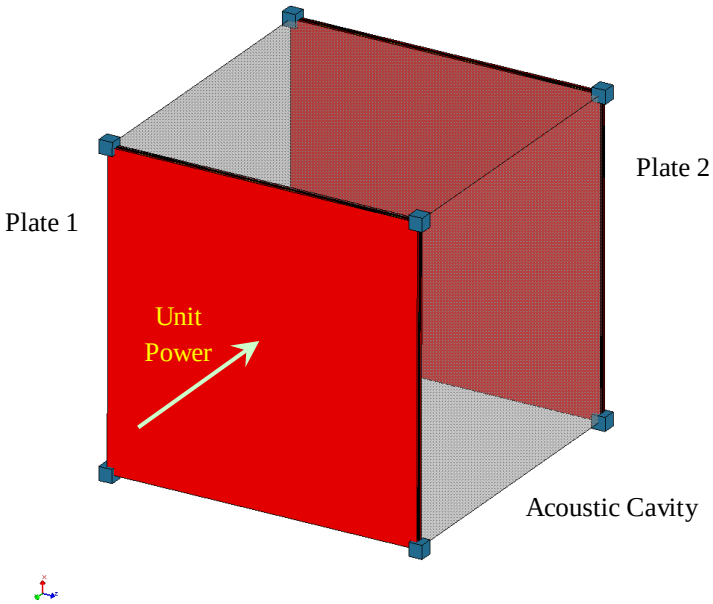

Figure 2. SEA cubical acoustic cavity model, featuring homogeneous parallel plates 1 and 2 on opposing sides, has a unit power applied to the center of plate 1.

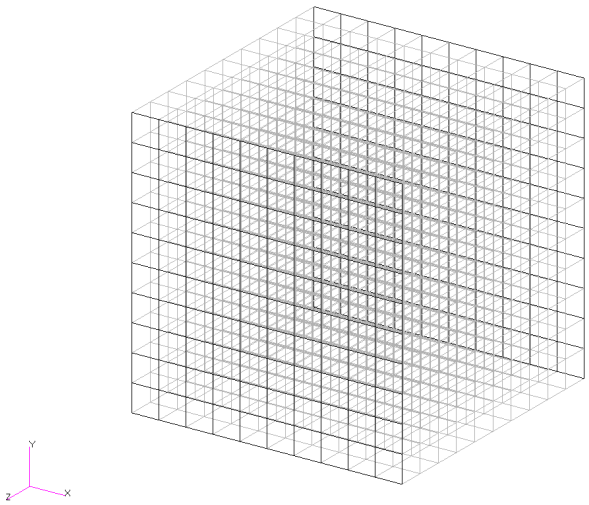

Figure 3. EFEA plate-cavity-plate finite element model.

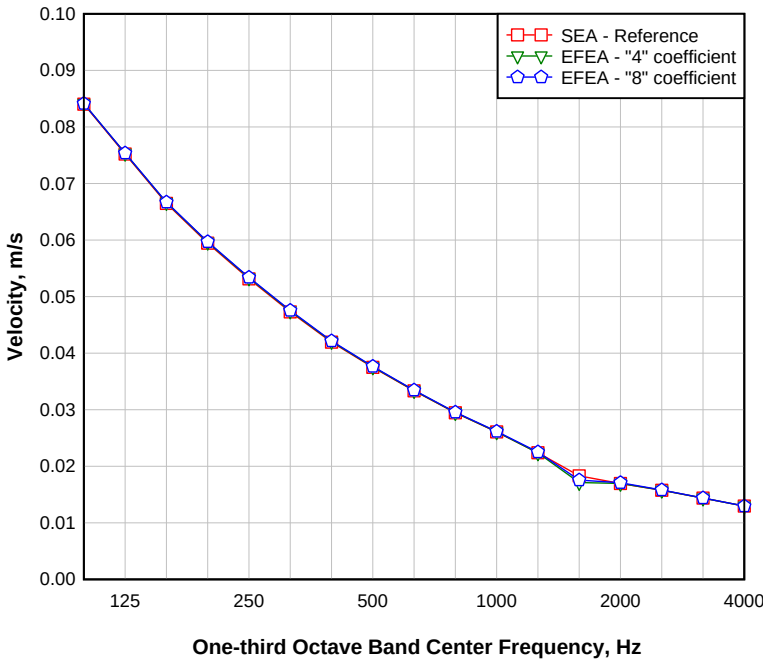

Figure 4. The root-mean-square velocity response of the excited plate 1 predicted by SEA, and by EFEA with the power transmission coefficients in Equation (5) with the "8" coefficient and Equation (6) with the "4" coefficient.

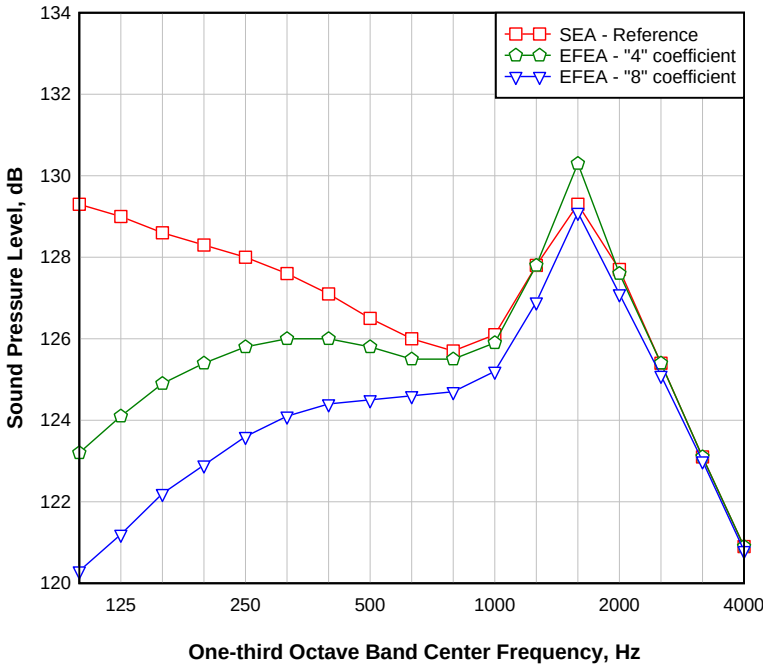

Figure 5. The sound pressure level response of the acoustic cavity predicted by SEA, and by EFEA with the power transmission coefficients in Equation (5) with the "8" coefficient and Equation (6) with the "4" coefficient.

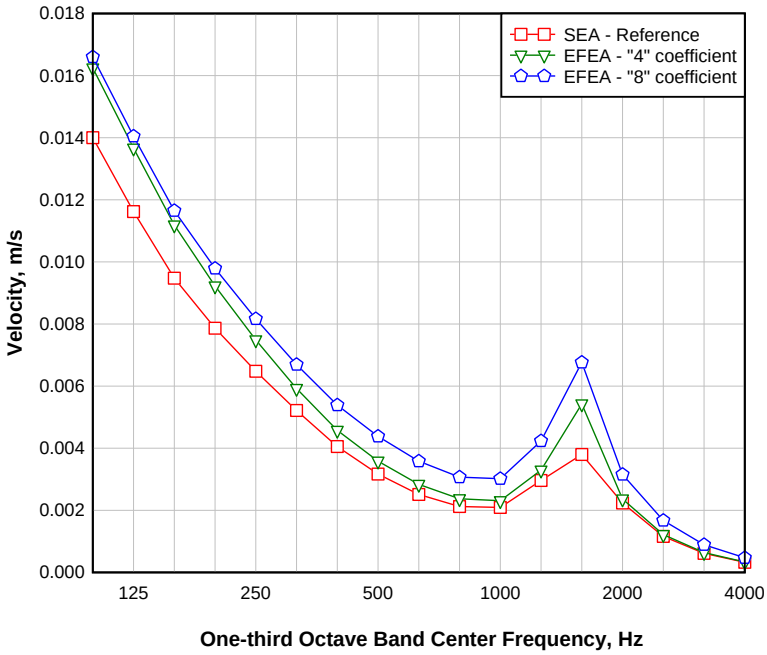

Figure 6. The root-mean-square velocity response of the opposing plate 2 predicted by SEA, and by EFEA with the power transmission coefficients in Equation (5) with the "8" coefficient and Equation (6) with the "4" coefficient.

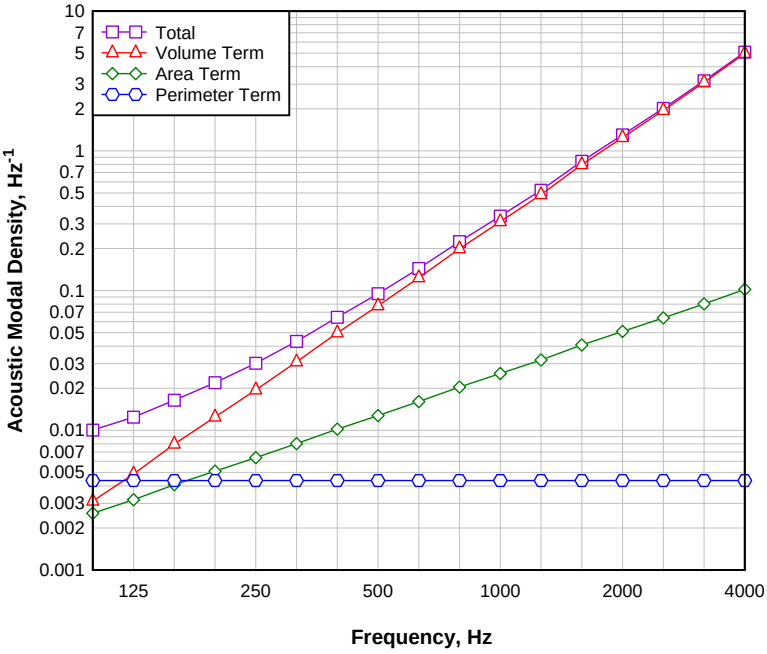

Figure 7. Acoustic modal density predicted using the Volume (EFEA), the Area or the Perimeter term or a combination of all three (Total).

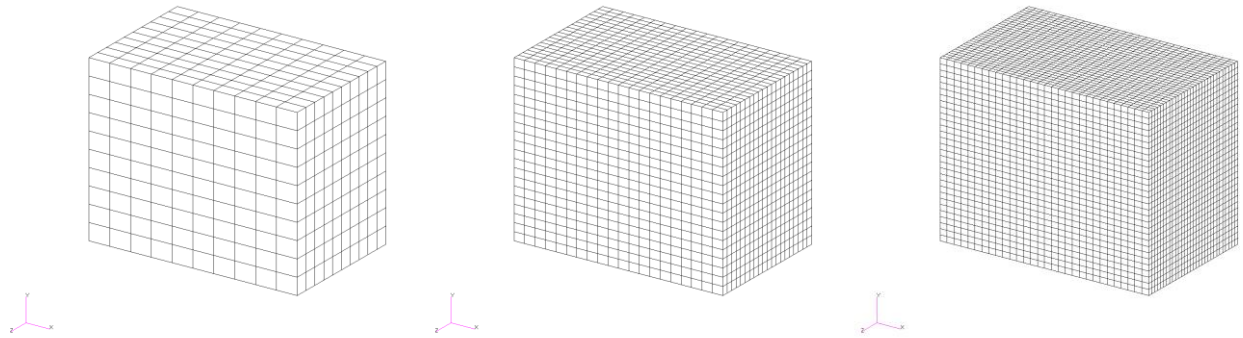

a) b) c)

Figure 8. Hidden line finite element models of the rectangular acoustic cavity with ten, twenty, thirty elements per length, width or height dimension.

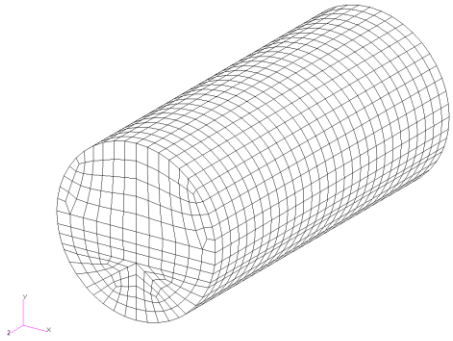

Figure 9. Hidden line finite element model of the cylindrical acoustic cavity with length l and radius r.

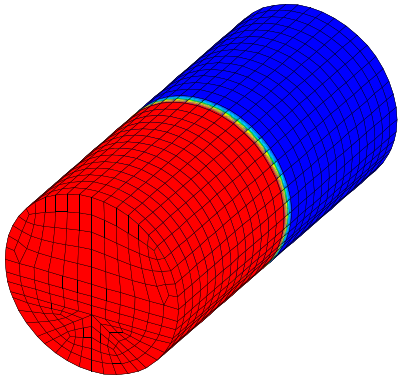

Figure 10. Phase plot of the numerical fundamental longitudinal acoustic mode (0,0,1) in the cylinder cavity at 46.9 Hz (Table 8).

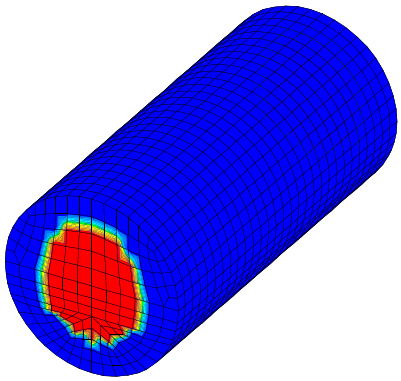

Figure 11. Phase plot of the numerical fundamental radial acoustic mode (1,0,0) at 246.2 Hz in the cylinder cavity (Table 8).

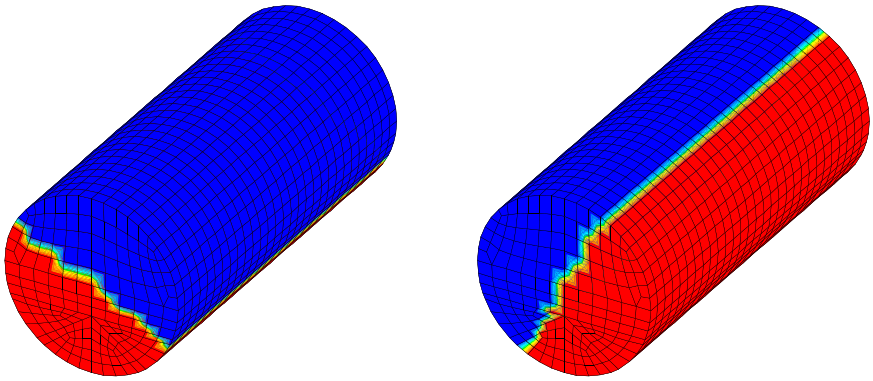

a) b)

Figure 12. Phase plot of the numerical fundamental azimuthal acoustic mode (0,1,0) at 119.6 Hz and the same mode shape at a relative 90° phase rotation (119.7 Hz) in the cylinder cavity (Table 8).

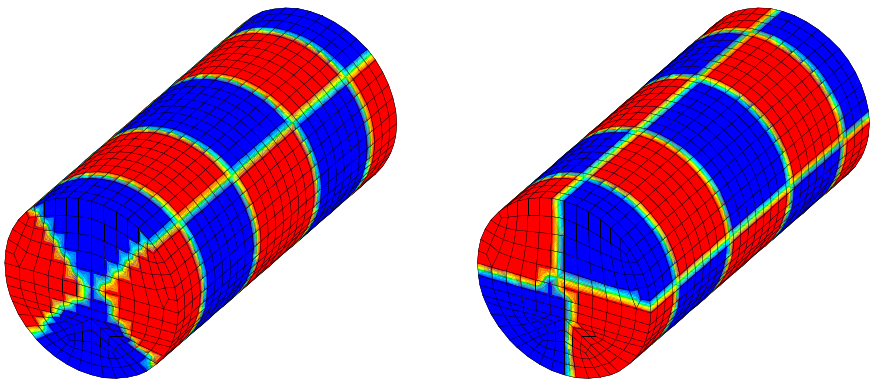

a) b)

Figure 13. Phase plot of the (0,2,4) azimuthal- longitudinal acoustic mode at 266.6 Hz and the same mode shape at 45° relative phase rotation (266.9 Hz) in the cylinder cavity.

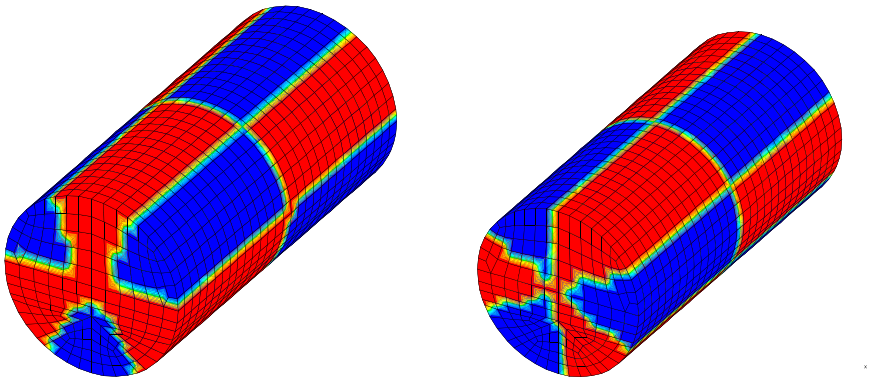

a) b)

Figure 14. Phase plot of the (0,3,1) azimuthal- longitudinal acoustic mode at 272.3 Hz and the same mode shape at 30° relative phase rotation (272.8 Hz) in the cylinder cavity.

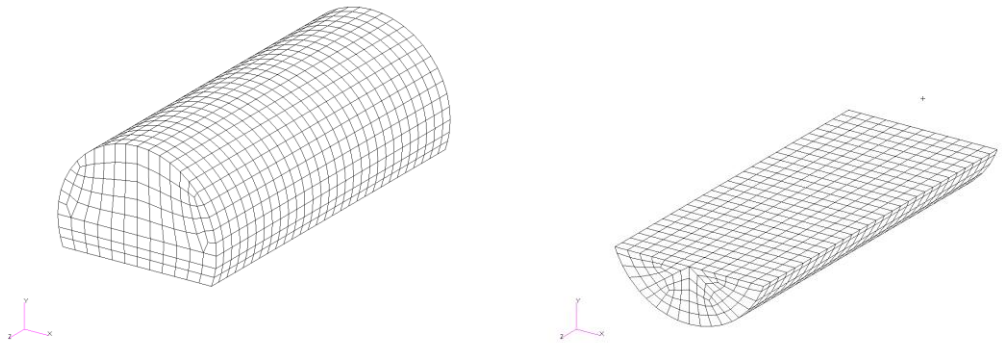

a) b)

Figure 15. Hidden line finite element models of the cylinder acoustic cavity, the top part of the cylinder above the floor and the bottom part below the floor.

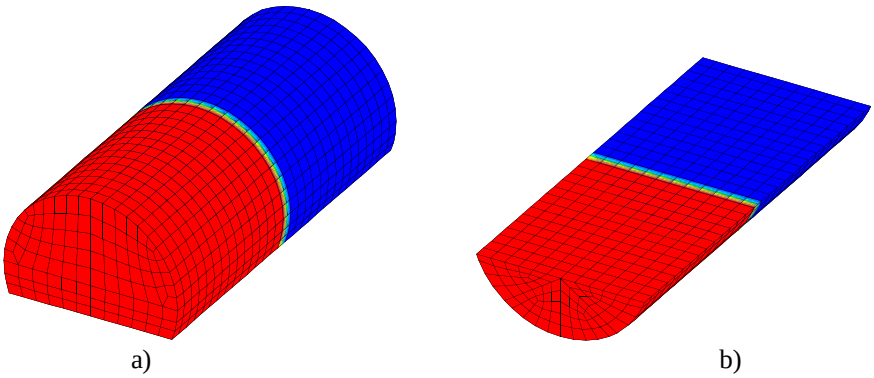

a) b)

Figure 16. Phase plot of the numerical fundamental longitudinal acoustic mode at 46.9 Hz in the cavity above the floor (Table 14) and the cavity below the floor (Table 15).

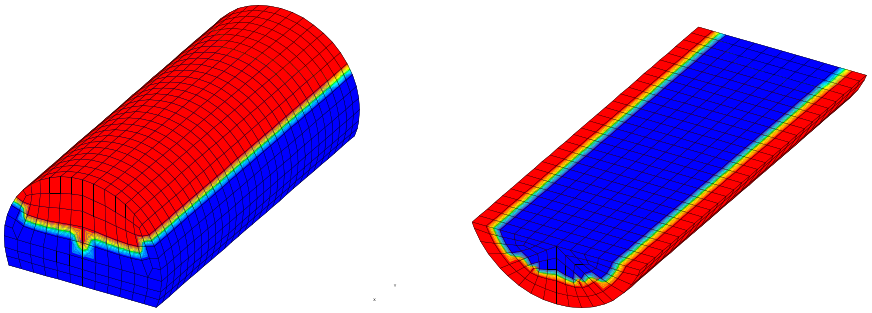

a) b)

Figure 17. Phase plot of the numerical fundamental radial acoustic mode at 160.3 Hz in the cavity above the floor (Table 14) and at 351.2 Hz in the cavity below the floor (Table 15).

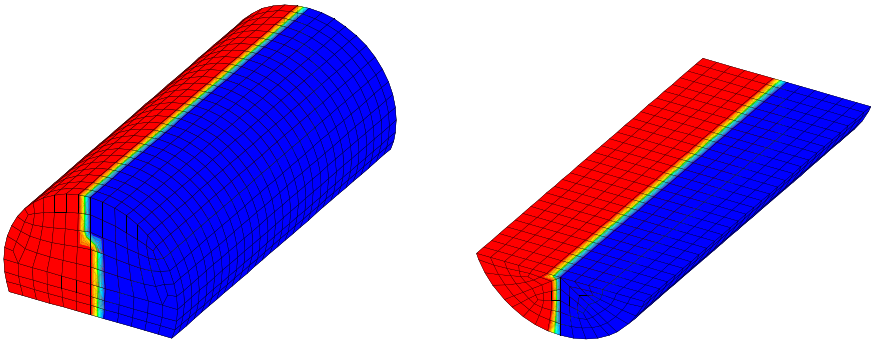

a) b)

Figure 18. Phase plot of the numerical fundamental azimuthal acoustic mode at 113.8 Hz in the cylinder cavity above the floor (Table 14) and at 137.5 Hz in the cavity below the floor (Table 15).

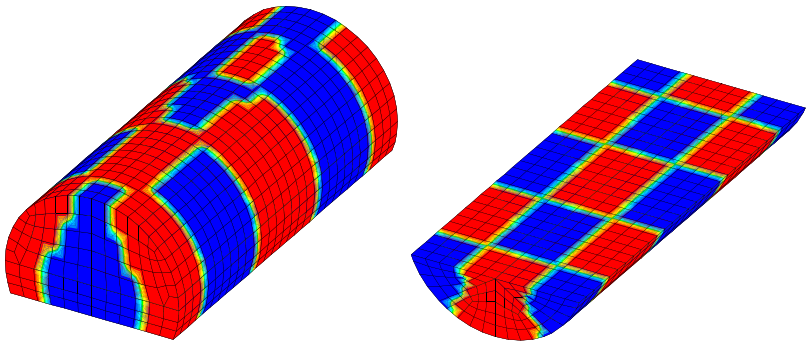

a) b)

Figure 19. Phase plot of the (0,2,4) azimuthal- longitudinal acoustic mode at 282.0 Hz in the cylinder cavity above the floor (Table 14) and at 296.8 Hz in the cavity below the floor (Table 15).

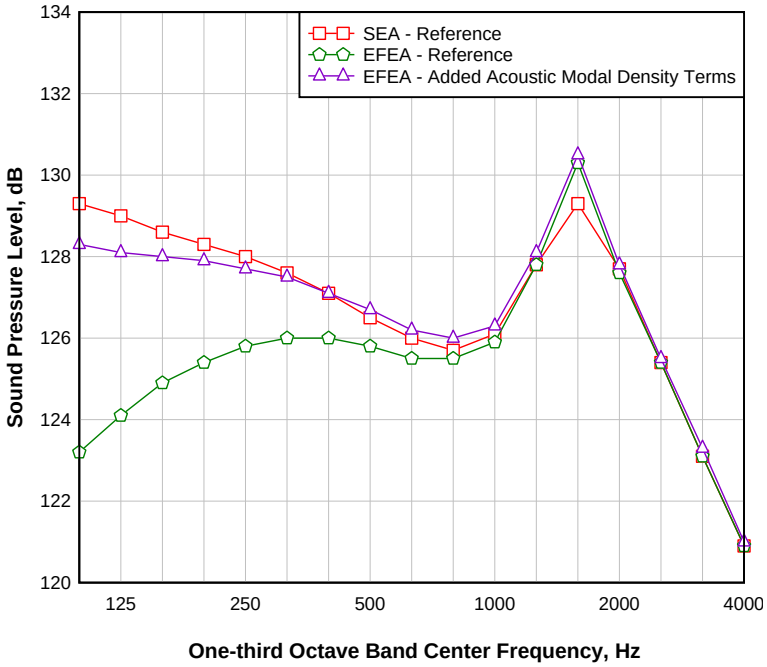

Figure 20. Acoustic cavity sound pressure level predictions by SEA, EFEA with only the volume term (Reference), and EFEA with the area and perimeter terms added to the volume term.

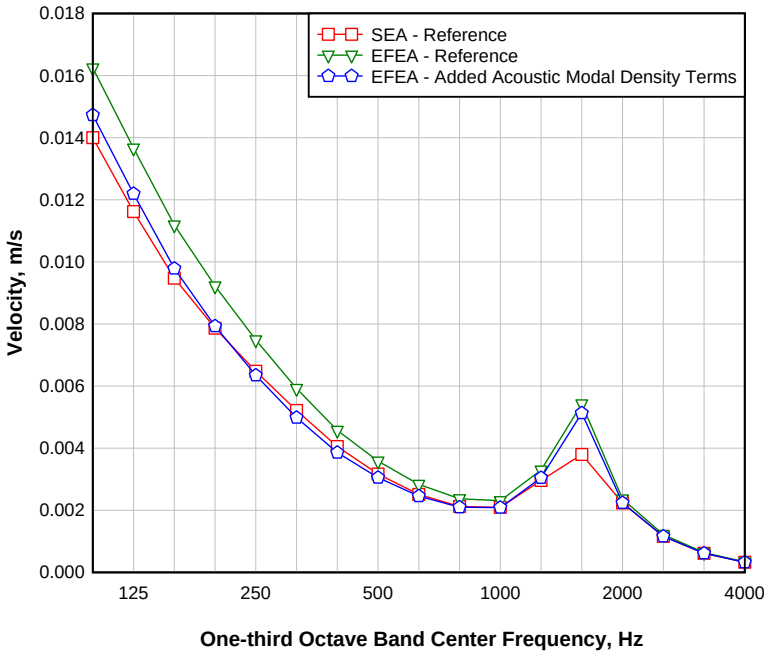

Figure 21. Plate 2 root-mean-square velocity predictions by SEA, EFEA with only the volume term (Reference), and EFEA with the area and perimeter terms added to the volume term.

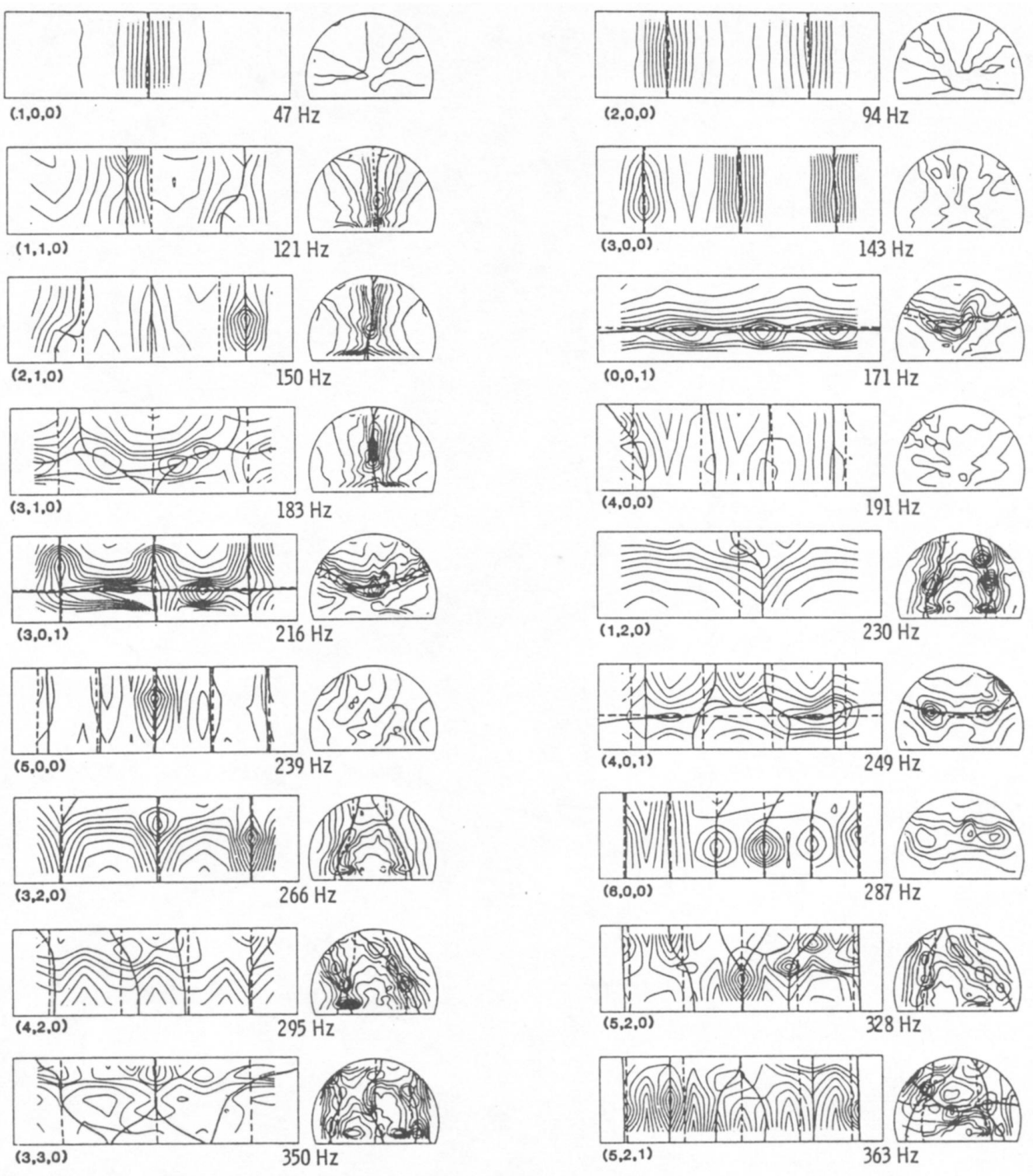

Figure 22. Measured and calculated modal parameters for the cavity above the floor of the composite cylinder (Reference 1).

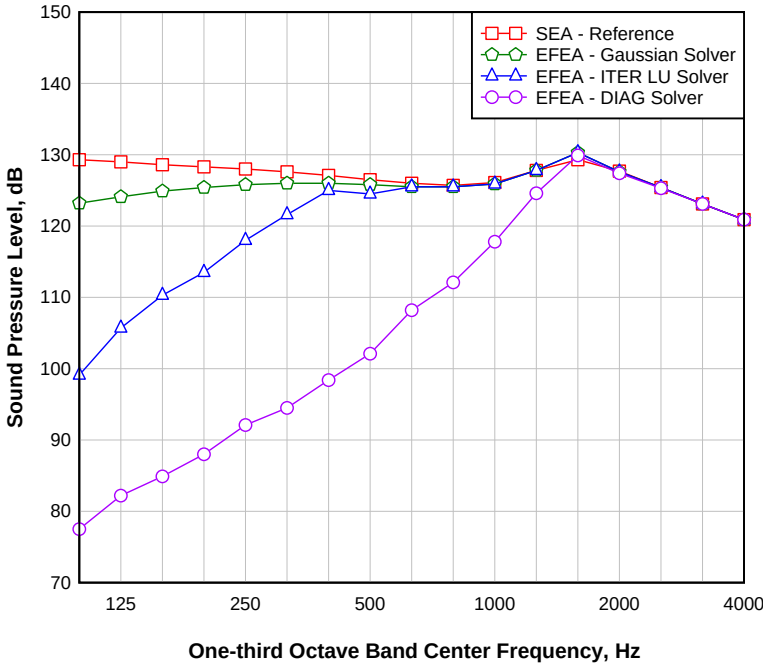

Figure 23. SEA acoustic sound pressure level predictions compared with EFEA results using the default Gaussian Elimination solver, the optional Incomplete LU (ITER LU) or the Diagonal Scaling (DIAG) solver.

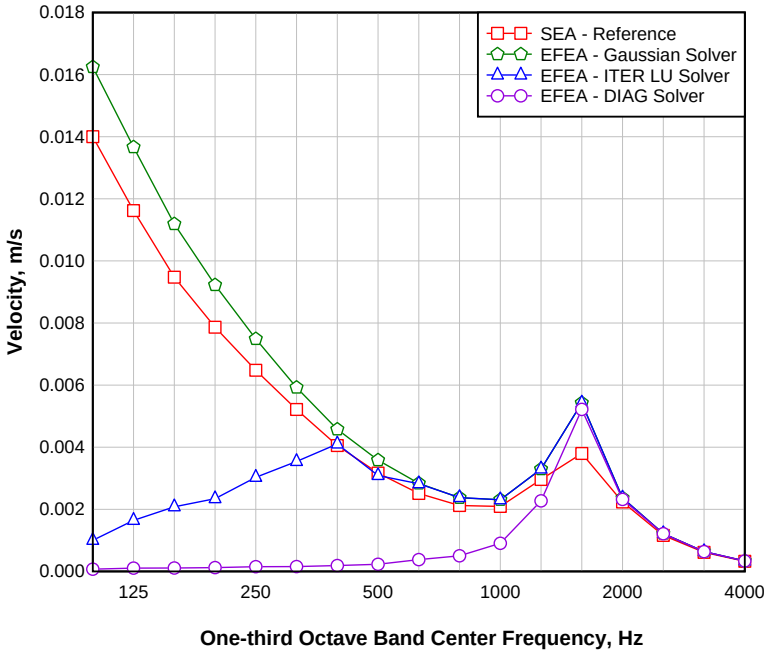

Figure 24. SEA plate 2 root-mean-square velocity predictions compared with EFEA results using the default Gaussian Elimination solver, the optional Incomplete LU (ITER LU) or the Diagonal Scaling (DIAG) solver.

REPORT DOCUMENTATION PAGE

Form Approved
OMB No. 0704-0188

1. REPORT DATE *(DD-MM-YYYY)*	2. REPORT TYPE	3. DATES COVERED *(From - To)*
01- 02 - 2010	Technical Memorandum	

4. TITLE AND SUBTITLE

Comparison of Comet Enflow and VA One Acoustic-to-Structure Power Flow Predictions

5a. CONTRACT NUMBER

5b. GRANT NUMBER

5c. PROGRAM ELEMENT NUMBER

6. AUTHOR(S)

Grosveld, Ferdinand W.; Schiller, Noah H.; Cabell, Randolph H.

5d. PROJECT NUMBER

5e. TASK NUMBER

5f. WORK UNIT NUMBER

877868.02.07.07.04.01

7. PERFORMING ORGANIZATION NAME(S) AND ADDRESS(ES)

NASA Langley Research Center
Hampton, VA 23681-2199

8. PERFORMING ORGANIZATION REPORT NUMBER

L-19820

9. SPONSORING/MONITORING AGENCY NAME(S) AND ADDRESS(ES)

National Aeronautics and Space Administration
Washington, DC 20546-0001

10. SPONSOR/MONITOR'S ACRONYM(S)

NASA

11. SPONSOR/MONITOR'S REPORT NUMBER(S)

NASA/TM-2010-216191

12. DISTRIBUTION/AVAILABILITY STATEMENT

Unclassified - Unlimited
Subject Category 71
Availability: NASA CASI (443) 757-5802

13. SUPPLEMENTARY NOTES

14. ABSTRACT

Comet Enflow is a commercially available, high frequency vibroacoustic analysis software based on the Energy Finite Element Analysis (EFEA). In this method the same finite element mesh used for structural and acoustic analysis can be employed for the high frequency solutions. Comet Enflow is being validated for a floor-equipped composite cylinder by comparing the EFEA vibroacoustic response predictions with Statistical Energy Analysis (SEA) results from the commercial software program VA One from ESI Group. Early in this program a number of discrepancies became apparent in the Enflow predicted response for the power flow from an acoustic space to a structural subsystem. The power flow anomalies were studied for a simple cubic, a rectangular and a cylindrical structural model connected to an acoustic cavity. The current investigation focuses on three specific discrepancies between the Comet Enflow and the VA One predictions: the Enflow power transmission coefficient relative to the VA One coupling loss factor; the importance of the accuracy of the acoustic modal density formulation used within Enflow; and the recommended use of fast solvers in Comet Enflow. The frequency region of interest for this study covers the one-third octave bands with center frequencies from 16 Hz to 4000 Hz.

15. SUBJECT TERMS

Acoustics; Energy Finite Element Analysis (EFEA); Statistical Energy Analysis (SEA); Power transmission coefficient; Coupling loss factor; Acoustic modal density

16. SECURITY CLASSIFICATION OF:			17. LIMITATION OF ABSTRACT	18. NUMBER OF PAGES	19a. NAME OF RESPONSIBLE PERSON
a. REPORT	b. ABSTRACT	c. THIS PAGE			STI Help Desk (email: help@sti.nasa.gov)
					19b. TELEPHONE NUMBER *(Include area code)*
U	U	U	UU	51	(443) 757-5802